

# Numerical Investigation of Seismic Performance of Reinforced Concrete Frame Strengthened With CFRP

Shimelis Getachew Tola

Department of Civil Engineering, College of Civil and Architectural Engineering Addis Ababa Science and Technology University, Addis Ababa, Ethiopia

**Email address:**

shimelis2015@gmail.com

**To cite this article:**

Shimelis Getachew Tola. (2023). Numerical Investigation of Seismic Performance of Reinforced Concrete Frame Strengthened With CFRP. *Engineering and Applied Sciences*, 8(5), 90-111. <https://doi.org/10.11648/j.eas.20230805.12>

**Received:** September 21, 2023; **Accepted:** October 28, 2023; **Published:** December 22, 2023

---

**Abstract:** Reinforced concrete (RC) structure performance behavior investigation is important in order to produce structural systems having stiffness, strength, deformation capacity required to withstand seismic loading with acceptable performance. Number of studies conducted to investigate the performance of structural RC frame members such as beams, columns, beam-column joints under seismic loading, primarily using experimental methods. The main aim of this thesis is to investigate numerically the performance of RC portal frame strengthened with 0%, 10%, 15%, 20%, 25% and 30% of total length of RC frames with carbon fiber reinforced polymer (CFRP) under seismic loading in displacement control. In the first scheme of this study finite element model for six RC portal frames strengthened with different percentages of CFRP have been developed by using finite element software called ABAQUS and those RC portal frames with identical dimension of beam and columns of cross section of 300x350mm and column is 1365mm in height and beam of 2350mm length has been simulated under seismic loads up to 3% drift ratio in displacement control. In the second schemes of this study finite element model for three RC portal frames (one as base lines and two were strengthened with CFRP sheets) subjected to lateral cyclic load and gravity loads on beam critical zones. Nonlinear finite element analysis with damaged plasticity model for concrete and orthographic elastic properties for CFRP in ABAQUS/standard is adapted to simulate RC portal frames. The accuracy of the nonlinear finite element models has been verified using the experiment results conducted on beam-column joints by other researchers. The Finite Element Analysis (FEA) results showed that strengthening the RC portal frame with the 10%, 15%, 20%, 25% and 30% of CFRP increased the dissipation energy capacity by 2.39%, 4.1%, 5.95%, 7.04% and 7.39% respectively. Results also showed that strengthening with CFRP results in fewer cracks, less degradation of strength after yielding than bare RC frame and decrease in stiffness degradation.

**Keywords:** RC Portal Frames, Carbon Fiber Reinforced Polymer, Finite Element Analysis, Seismic Loading and Displacement Control

---

## 1. Introduction

### 1.1. Background

Seismic assessment and reinforced concrete structure design are crucial to minimize damage from earthquakes [10, 15, 39]. Strengthening with carbon fiber reinforced polymer (CFRP) is key to optimizing seismic performance. Structural layouts should achieve high survival probability under seismic loads, as deformations and stresses induced by seismic effects vary [11, 22]. Performance-based engineering, developed after the 1994 Northridge earthquake, aims to

improve seismic monitoring in earthquake buildings by designing structures that anticipate seismic loading [5, 16, 23, 36, 37]. This process involves understanding the structure's optimal performance and selecting scenarios that align with structural function objectives, demonstrating design performance through analysis, simulation, testing, or combining. Some classical methods of retrofitting, such as concrete or steel column jacketing, the addition of shear walls, and methods often based on new materials such as fiber-reinforced polymers (FRP), can be implemented considering the required performance levels and to minimize the chance of failure and minimize costs and/or minimize

losses [3, 5, 32, 44]. In order to develop seismic fragility [9, 21, 33, 43] and earthquake damage estimates [1, 18, 24, 34], the performance-based assessment model has been a consistent research trend in the earthquake engineering community over the past two decades. The performance-based design philosophy enables engineers at a local site to evaluate a specific level of structural performance for a given level of earthquake hazard. Using recorded ground motions, nonlinear dynamic analytical procedures can be used for probabilistic seismic evaluation [19, 28]. High seismicity areas require ductile design principles for structural design, with high-strength concrete commonly used in high-rise buildings to minimize structural weight and withstand higher loads. However, increased brittleness and decreased deformation potential limit its use. Fiber-reinforced polymer (FRP) offers advantages like high strength, elasticity, light weight, corrosion resistance, fatigue resistance, and easy construction [7, 14, 17, 25, 31, 38, 42, 40]. Flexural strengthening of reinforced concrete members subject to monotonic loading has been successful, but further evaluation and studies are needed.

### 1.2. Statement of the Problems

To ensure the high performance capacity of RC frame subjected to seismic loading, it is important to investigate the structural performance of RC frame strengthened with different percentage of CFRP. Because the number of studies conducted to investigate the performance of structural RC frame such as beams, columns, beam-column joints under seismic loading, primary by using experimental methods [27]. While a large number of studies have been performed on the action of the reinforced concrete beam column joints retrofitting with FRP materials, minimal investigation considered the overall seismic activity of strengthened frames. This recognized on the basis of previous studies that most researchers were experimentally investigating the behavior of RC frames strengthened with different methods. In this study, numerical studies on portal frames strengthened with different percentages of CFRP basically at the joints and mid-span of columns and beam is carried out.

### 1.3. Objectives of the Research

The main objective of this thesis is to investigate the performance of reinforced concrete (RC) frames strengthened with CFRP under cyclic loading by using ABAQUS.

The specific objectives of this study can be summarized as follows:

1. To predict the load-displacement response of RC frame generated by using ABAQUS,
2. To assess the overall behavior of RC frame strengthened with different percentages of CFRP in terms of strength, energy dissipation, ductility and stiffness by using nonlinear finite element analysis,
3. To generate the load-drift ratio envelope curves in order to predict the behavior of RC frame subjected to cyclic loading by using ABAQUS,

4. To investigate the failure mechanisms and crack patterns of un-strengthened and strengthened RC portal frames under cyclic loading using nonlinear finite element analysis, and
5. To assess the influence of gravity loads on hysteretic behavior of RC portal frames subjected to cyclic loading.

### 1.4. Significance of the Study

This study aims to boost awareness of CFRP in construction to enhance seismic performance of RC frames, aiding research and design, and improving understanding of failure mechanisms, resulting in safer and cost-effective solutions.

### 1.5. Scope of the Study

The scope of the research provided in this document is limited to the structural performance of a single span and single-story RC portal frame strengthened with CFRP sheets subjected to quasi-static seismic loading in displacement control and gravity load at beam critical zones. ABAQUS software has been used to analyze and model 3-D portal frame structure.

### 1.6. Limitation of the Study

This study is limited to nonlinear finite element investigation performance of bare RC frame and RC frames strengthened with CFRP under cyclic loading with damaged plasticity model using embedded (perfect bond) method to simulate the bond between concrete and reinforcements. The accuracy of the nonlinear finite element models of bare RC and strengthened RC frame under cyclic loading have been validated with the available experimental results from the recent existing experimental study. The loading protocol in this study only consider displacement control cyclic loads as the lateral loads and gravity loads as vertical point loads, no other types of are used to study the response of the structures.

## 2. Methodology

### 2.1. General

The paper discusses the use of the CDP (concrete damaged plasticity) model for simulating nonlinear behavior of reinforced concrete structures under quasi-static loads. This model, a continuum, plasticity-based damage model, provides a general capability for modeling concrete. It details the material properties, element types, geometry, boundary conditions, loading, mesh and analyzes types used for modeling the RC frame in ABAQUS, and the process of strengthening the RC frame with CFRP.

### 2.2. Experimental work Description for Model Validation

In order to validate the numerical model, an experimental work from the literature is used. A beam column joint tested under cyclic loading by [13] is used in this paper. The

geometric characteristics of the models and material properties are considered in the experimental work carried out by [13]. This was a reinforced concrete frame of columns with a cross-section of 300x350 mm and a height of 1365 mm and a cross-section of a beam of 300x350 mm and 2350 mm length. In all specimens, the beams and columns were reinforced with the top and bottom bars of 2 $\Phi$ 16 mm. In the columns, beam and beam-column joint, the steel stirrups consisted of 10 mm bars at 100 mm c / c spacing. The whole specimen will be fitted with a clear cover of 25 mm (figure 1).

Compressive strength of the concrete was 30 MPa at 28 days age and the yield strength of reinforcement was 500 MPa.

*E.I. Saqan et al.*

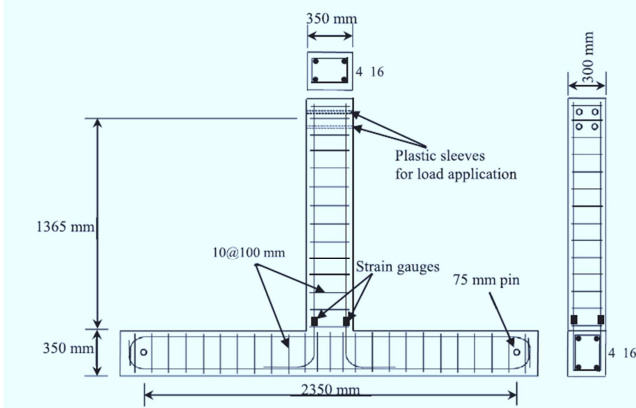


**Figure 1.** Overall dimensions and reinforcement details for Experimental specimen [13].

In order to make a baseline evaluation the sample was simulated in this study. Hence, many researchers were focused on the beam column joint performance analysis, this thesis aimed to investigate the whole response of RC frames subjected to cyclic loading which is modeled by using the same material properties used for experimental study of beam column joint specimen [6, 35]. The specimens were tested under cyclic loading which is applied at the tip of the column using a hydraulic actuator as shown in Figure 2. The specimens were analyzed under displacement control reversed cyclic loading procedure.

Generally, beam-column joint specimen which was experimentally tested by [13] is numerically modeled and validated against experimental results in validation section of

this study.

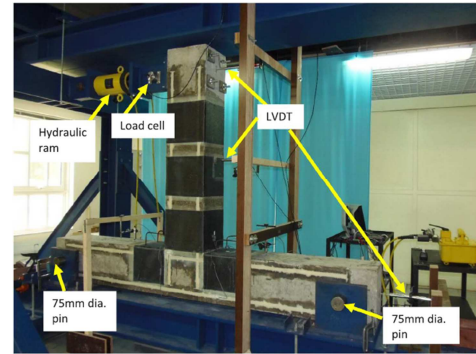


**Figure 2.** Test setup [13].

### 2.3. Description of Specimens for Numerical Study

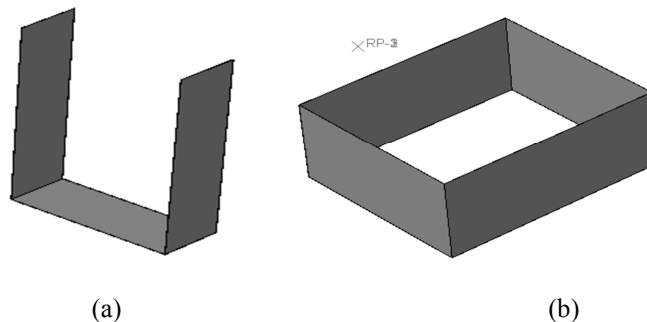
Nine RC portal frames under two schemes were modeled as the following:

In the first schemes, CFRP sheets were bonded to RC frames (columns and beam) at near to the beam column joints and for the sixth frame addition CFRP at beam center and all these six assemblages were subjected to cyclic lateral load histories to simulate loading.

1. One control frame model with 0% of CFRP
2. The other five model are reinforced with 10%, 15%, 20%, 25% and 30% of one layer of CFRP externally bonded four sides of columns and U-wraps of the flexural CFRP used to tie on the beam.

In the second schemes, three RC portal frames, one as baseline model and other two were strengthened with CFRP sheets under different configurations were developed and subjected to cyclic lateral load histories and gravity loads at the critical point of beams.

1. The first model of this part was bare RC frame which used as the base line (control) model,
2. The second model in this part was similar to 10% strengthened RC frame of the first schemes and their difference is only loading protocol, and
3. The third model in this part was CFRP sheets bonded at the bottom of column near to the fixed support of the RC frames added on the 10% strengthened RC frame of the first schemes.

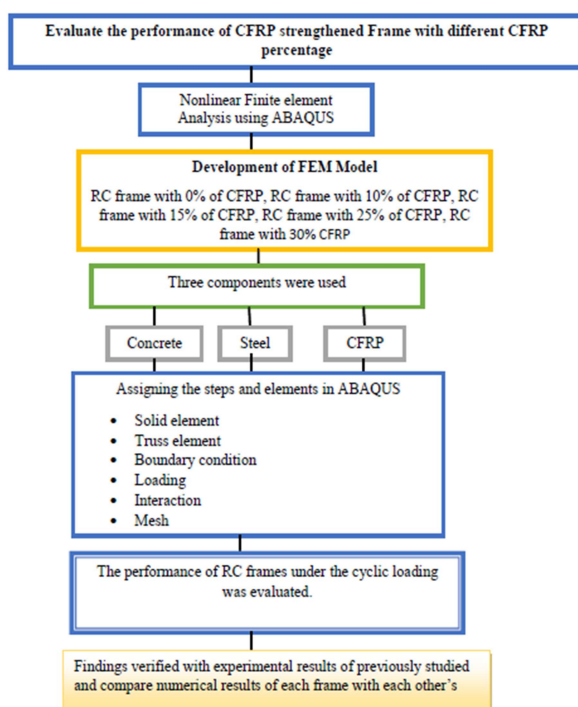


**Figure 3.** CFRP shape model: (a) flexural CFRP used to tie on the beam. (b) externally bonded CFRP for columns.

**Table 1.** Beam and Columns Dimensions Used to Modeling RC Frame with Their CFRP Percentage.

case	CFRP (%)	Name	Beam and columns dimensions (mm)	CFRP length (mm)	
				For each column	For beam(in both directions)
1	0	RCFB	300x350	-	-
2	10	RCF10	300x350	136.5	117.5
3	15	RCF15	300x350	204.75	176.25
4	20	RCF20	300x350	273	235
5	25	RCF25	300x350	341.25	587.5
6	30	RCF30	300x350	350 (provide at 300mm space at two positions with 350mm)	235 (provided at the edges and at middle of beam)

The materials properties and reinforcement detail used for validation is also used for RC portal frames of this study. In this study, finite element modeling will focus on concrete modeling, steel reinforcement, CFRP and interaction between the different elements.

**Figure 4.** Schematic diagram for the NLFEM of RC frames.

## 2.4. Finite Element Modeling in ABAQUS

This study uses ABAQUS, a powerful finite element method software, for nonlinear finite element analysis of structural members. The software offers a wide range of

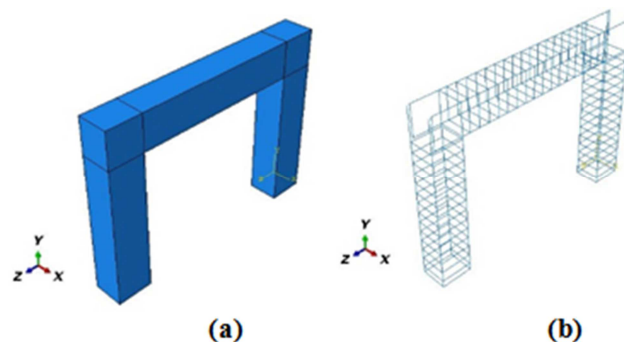
nonlinear material models and can simulate one, two, and three-dimensional models [29]. It includes three major products: ABAQUS/CAE, ABAQUS/Standard, and ABAQUS/Explicit. ABAQUS/CAE allows for creating, analyzing, and visualizing model output in one environment. In this study, three-dimensional (3-D) non-linear finite element analyzes of reinforced concrete (RC) frames and RC frames strengthened with carbon fiber reinforced polymer (CFRP) are performed using ABAQUS/Standard. The three-dimensional Finite Element models of reinforced concrete frames have been developed on the basis of the central objectives of this research and the various elements concerned with modeling are addressed as follows.

1. Elements type
2. Material property
3. Assigning sections
4. Defining step
5. Interaction between elements
6. Specify boundary conditions and load
7. Meshing
8. Assigning job
9. Evaluating the results

### 2.4.1. Element Type and Interactions between Components

#### Element Types

This paper presents a numerical simulation of a reinforced concrete (RC) structure using concrete, steel, and CFRP materials. The study uses ABAQUS to create a 3D solid element with eight nodes and three degrees of freedom, which can be extruded in any direction [8]. The CFRP is modeled using a three-dimensional two nodes first-order truss element. The element is capable of plastic deformation, cracking in three orthogonal directions, and crushing.

**Figure 5.** FEM geometry (a), Overall assembly of model parts, (b) Reinforcement cage.



#### 2.4.2. Boundary Conditions and Constraints

The proper modelling of boundary conditions in ABAQUS/ Standard is considered one of the most important parts of the model.

The type of boundary condition for all degree of freedom is defined as a fixed boundary condition at the bottom of the columns ( $U_1=U_2=U_3=UR_1=UR_2=UR_3=0$ ). That's mean

that the movement in all direction will be restricted. The load is applied as uniform displacement load to the top of the frame in z-direction ( $U_3=1$ ). Figure 6 shows the boundary condition and load location for the model. The amplitude of displacement applied was 51.14 mm by [13] as show in Figure 6.

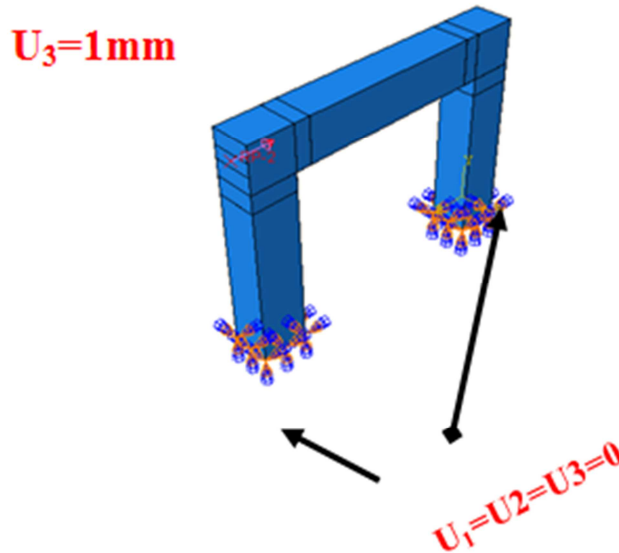


Figure 6. Boundary conditions and loading

#### 2.4.3. Cyclic Loading Protocol

The loading applied to the top of the column frame consists of quasi-static lateral displacement based cycles controlled. Figure 7 shows the loading applied for FEA of RC frame. For three cycles per drift, initial cycles to start with  $\pm 0.05$  percent and  $\pm 0.1$  percent lateral drift are completed. Such cycles were within the elastic range which allowed the frame to be stiff and displaced. Subsequent intervals consisting of three large amplitudes with a  $\pm 0.05$

percent increase in drift. The lateral displacement was applied slowly and steadily in order to obtain the pattern of hysteresis loops. Up to 3 percent lateral drift was achieved in this cycle. The damage will defined on the basis of cracks, concrete pouring, and support bar buckling & bar fracture. The lateral displacement and loading was applied at 1715 mm height. The cyclic loading was repeated three times at each drift ratio value.

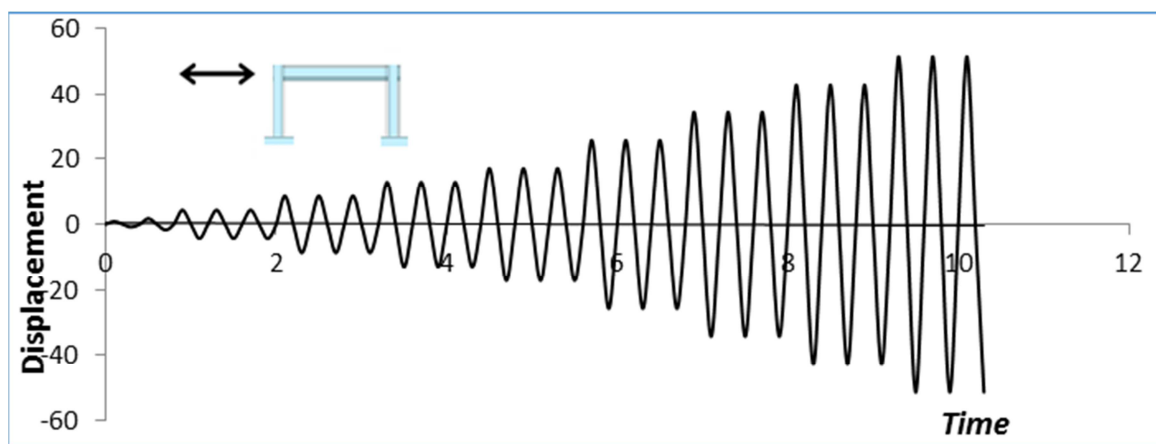


Figure 7. Displacement-controlled loading procedure [13].

For the second part the gravity load which is 75% of the first yield of the bare RC frame of the first part which is

104.38 KN was applied on the beam critical zone.

#### 2.4.4. Material Modeling

##### (i). Modeling of Steel Reinforcement

The steel Reinforcement (longitudinal and transverse), using embedding technique, will be modeled as a truss element embedded in concrete assuming a perfect bond

between the steel and concrete. If truss element is used for steel reinforcement, when subject to multi-axial stress, it is unnecessary to consider steel's complex behavior. Therefore, under tension and/or compression, a perfect elasto-plastic is used to idealize the stress curve.

**Table 2.** Mechanical properties of steel used in FE modeling.

Yield strength (MPa)	Mass density (tone/mm3)	Elastic modulus (MPa)	Poisson's ratio
500	7.85E-009	210000	0.3

##### (ii) CFRP Modeling

FRPs ' behavior depends on their mechanical properties, fiber orientation, length, shape and constituent fibers, epoxy adhesive properties, and the nature of their bonded surface.

Usually, FRPs display linear elastic properties without inelastic deformation until failure. The orthotropic plane stress failure of FRPs is represented by many proposed theories.

**Table 3.** Mechanical properties of the CFRP fibers.

Fiber Type	Nominal Thickness or Diameter t,d (mm)	Ultimatetensile strength $f_{tu}$ (MPa)	Elongation at break $\epsilon_{fu}$ (%)	Modulus of elasticity E (GPa)
Carbon Dry Fiber	0.33	4830	2.1	227.5

CFRP wraps are defined as shell homogenous with a thickness of value of 0.33mm using three points Gauss integration rule for analysis. The CFRP composite strip was modelled as an orthotropic elastic material and it has linear behavior up to failure. The stress-strain relationships can be expressed thus;

Where the stiffness matrix consists of nine independent elastic stiffness parameters ( $D_{ijk}$ ), which were defined as shown in Equations (5.9)-(5.16) (ABAQUS, 2011).

The orthotropic properties of the cured CFRP

The behavior of the composite sheet can be represented through a set of orthotropic constitutive relations. In the orthotropic elastic model a set of such relationships are described which assume the material behavior remains elastic and the volumetric response linear. CFRP is a uniaxial and brittle material with a linear stress-strain relationship up to fail. The nominal properties of the CFRP sheet as per suppliers and reported from literature are presented in table 3.4.

The material data required for modeling of the property of carbon fiber reinforced polymer sheet is listed below:

1. Orthotropic Young's Modulus:-( $E_1$ : in-plane, in the fiber direction,  $E_2$ : In-plane, orthogonal to the fiber direction,  $E_3$ : out of plane direction)
2. Orthotropic Poisson's Ratio:- ( $\nu_{12}$ : In-plane,  $\nu_{13}$ : out of the plane, in the fiber direction,  $\nu_{23}$ : out of the plane, normal to fiber direction)
3. Orthotropic Shear Modulus:-( $G_{12}$ : In-plane,  $G_{13}$ : out

of the plane, in the fiber direction,  $G_{23}$ : out of the plane, normal to fiber direction).

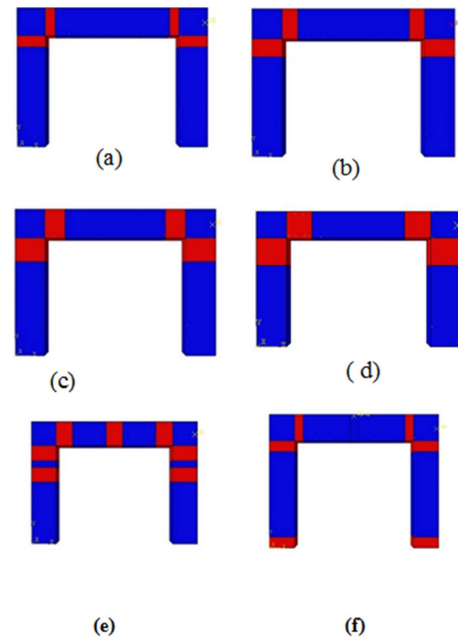


**Figure 8.** CFRP configurations, (a) RC frame strengthened with 10% of CFRP (RCF10), (b) RC frame strengthened with 15% of CFRP (RCF15), (c) RC frame strengthened with 20% of CFRP (RCF20), (d) RC frame strengthened with 25% of CFRP (RCF25), (e) RC frame strengthened with 30% of CFRP (RCF30), (f) RC frame strengthened with additional CFRP sheets at the bottom of the column.

**Table 4.** CFRP elastic orthotropic properties.

Abaqus parameters	D1111	D2222	D3333	D1122	D1133	D2233	D1212	D1313	D2323
CFRP(Mpa)	138660	13604	13604	6101	6101	6937	5000	5000	1940

##### (iii) Concrete Modeling

ABAQUS/standard has two approaches to model concrete

behavior; smeared cracking and damaged plasticity. The smeared crack concrete model offers a general ability for modeling concrete in different types of concrete structures

including trusses, beams, shells and solids. This model does not track individual macro-cracks during analysis. It has difficulty to making the model suitable in 3D applications due to the convergence problems which are caused by non-existence of cyclic/unloading response or the damage in the elastic stiffness resulting from plastic straining. Otherwise, the damaged plasticity model is mostly used in structures subjected to cyclic or dynamic loading because it is capable to anticipate the behavior of the simulation up to failure. For the reason outline above, the damaged plasticity model has chosen for analysis each RC frames.

#### 2.4.5. Principles of the Concrete Damaged Plasticity

The most significant aspects of the damaged plasticity model can be defined as compression and tension degradation. When the element plasticizes, the elastic stiffness becomes lowered by damaged properties, thus it is

unable to recover its initial elastic stiffness. This is substantial for cyclic loading, as the two damage parameters,  $d_t$  and  $d_c$ , which are assumed to be functions of plastic strains, temperature and field variables represent degradations of elastic stiffness.

$$d_t = d_t(\epsilon_t^{pl}, \theta, f_i); 0 \leq d_t \leq 1$$

$$d_c = d_c(\epsilon_c^{pl}, \theta, f_i); 0 \leq d_c \leq 1$$

Where the subscripts t and c refer to tension and compression respectively; and are the equivalent plastic strains; is the temperature; and are other predefined field variables (ABAQUS, 2011). The damage parameters can take values ranging from zero (characterizing the undamaged material), to one (characterizes total loss of strength). The default of damage plasticity can be illustrated using Figure 9.

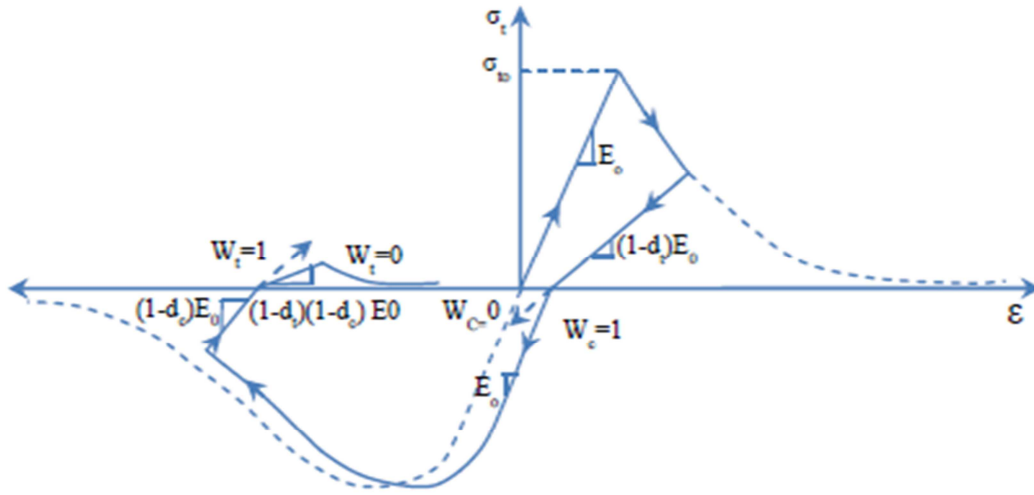


Figure 9. Uniaxial load cycle (tension-compression-tension) [2].

#### Compressive behavior

According to [4] the concrete stress-strain behavior under compression was modeled in three phases using formulation given in [20], and [2, 41] with some modifications.

Phase I: This stage represents the linear-elastic branch in which  $\epsilon_c$  is variable changing from zero to a  $0.4f'_c/E_c$  and  $E_c$  is the initial modulus of elasticity. The linear branch ends at the stress level of 40 percent of  $f'_c$  i.e  $0.4 f'_c$ .

$$\sigma_{c,1} = E_c \epsilon_c, E_c \leq 0.4 f'_c / E_c$$

Phase II: This stage is the hardening phase. At this stage the stress increases gradually until it reaches a strain level of 0.0035. It describes the ascending branch of the stress strain relationship reaching the peak stress,  $\sigma_{cu}$  at corresponding strain level  $\epsilon_{c0} = 2f'_c / E_c$ , where  $\eta_c$  is material constant obtained from the relation of phase 1 and 2 which means from the stress and strain.

Compatibility at the strain level of  $E_c = 0.4 f'_c / E_c$ .

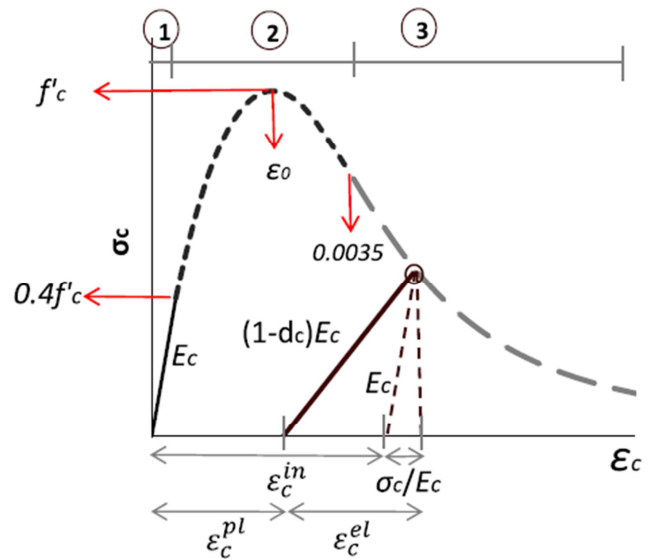


Figure 10. The uniaxial compressive stress-strain relationship for concrete [4].

Phase III: This stage is post peak softening phase. It represents the initiation and progression of compressive damage in the concrete material until the ultimate compressive strain  $\varepsilon_u$  attained. Using the stress-strain compatibility at the strain level of  $\varepsilon_c = 0.0035$ , for the second and third phase equations enables the value of  $\lambda_c$  (constant crushing energy as a material property) to be determined. The concrete ultimate strain  $\varepsilon_u$  was set to a large value of 0.035 to avoid any numerical difficulties.

$$\sigma_{c,2} = \frac{\eta_c \frac{\varepsilon_c - (\frac{\varepsilon_c}{\varepsilon_0})^2}{\varepsilon_0}}{1 + (\eta_c - 2) \frac{\varepsilon_c}{\varepsilon_0}} f'_c, 0.4 f'_c / E_c \leq \varepsilon_c \leq 0.0035$$

The ABAQUS uses data in terms of inelastic strain  $\varepsilon_c^{\text{in}} = \varepsilon_c - (\sigma_c / E_c)$ , which is total strains minus elastic strains corresponding to undamaged material.

Tensile behavior

In order to simulate the complete tensile behavior of reinforced concrete in ABAQUS, a post failure stress-strain relationship for concrete subjected to tension (similar to Figure 11) which is responsible for tension stiffening, strain-softening and reinforcement interaction with concrete.

To develop this model, young's modulus ( $E_0$ ), stress ( $\sigma$ ), cracking strain ( $\varepsilon_{t-ck}$  values and the damage parameter values ( $d$ ) for the relevant grade of concrete were used as input. The cracking strain ( $\varepsilon_{t-ck}$ ) should be calculated from the total strain using  $\varepsilon_{t-ck} = \varepsilon_t - \varepsilon_{t-el}$ , Where,  $\varepsilon_{t-el} = \sigma / E_0$ , the Elastic strain corresponding to the undamaged material,  $\varepsilon_t$  = total tensile strain.

According Modified Tension Stiffening Model for ABAQUS the concrete stress-strain behavior under tension was modeled in two phases.

$$\sigma_t^1 = E_c \varepsilon_t \text{ for } \varepsilon_t \leq \varepsilon_{cr}$$

$$\sigma_t^2 = f'_t \left( \frac{\varepsilon_{cr}}{\varepsilon_t} \right)^{0.4}, \text{ for } \varepsilon_t > \varepsilon_{cr}$$

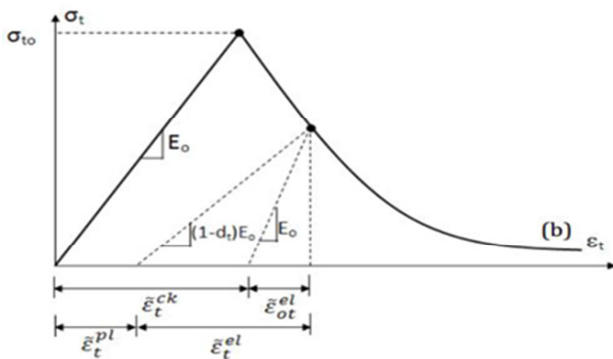


Figure 11. Stress-strain response for concrete in tension [2].

## 2.5. Parameters Calibrations

Calibration analyses in the finite element are often performed to quantify the effects of the varying material parameters on a numerical model by comparing the experimental and numerical results [4]. Hence, in order to

ensure the accuracy of the nonlinear finite element model of the RC frames, it is important to calibrate the effects of varying geometric and material input parameters such as mesh size, dilation angle and viscosity parameter in constitutive equations of damaged plasticity model.

### 2.5.1. Mesh Sensitivity

The meshing of the finite element model is an important phase of the numerical modelling which will determine the degree of accuracy of the outputs from the analysis. It is important to choose an appropriate dimension of the mesh for the model which gives a converged solution. For this study, 100mm mesh size are used for RC frame (Figure 12).

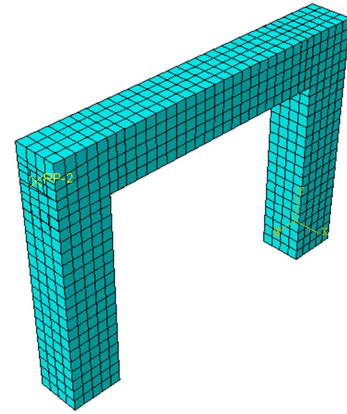


Figure 12. Frame meshing (ABAQUS).

### 2.5.2. Dilation Angle ( $\psi$ )

In the concrete damaged plasticity model, the change in volume of the quasi-brittle materials under compression (i.e. dilatancy) modelled by assigning a dilation angle value ( $\psi$ ). The dilatancy of concrete material characterizes the existence of expansion in volume when the material is exposed to triaxial stress and the consequent inelastic strain [30]. A range between 30° to 42° of the dilation angle parameters is recommended according to the studies performed by different authors [26, 30].

### 2.5.3. Viscoplastic Regularization

A viscosity parameter ( $\mu$ ), can be set to allow the material to temporarily exceed the plastic potential surface in order to handle convergence issues and to improve the solution, it is suggested to define a value close to 15% of the step time increment. However, regarding the high nonlinearity of the modelling of the joints, the time increment step was not fixed, and it was set automatically.

### 2.5.4. Shape Factor of the Yield Surface ( $KC$ )

According to the concrete damaged plasticity model in ABAQUS, the parameter  $KC$  is essential to define the shape of the yield surface and is ranged between 0.5 and 1, its default value of 0.667 (Simulia, 2017). For reinforced concrete structures according to finite element studies performed by different authors adopted the value of  $KC$  depending on the calibration study. For the present study, four different values of  $KC = 0.51, 0.667, 0.8$  and  $0.9$ , are



taken for examination.

**Table 5.** Concrete damage plasticity (CDP) input parameters.

Dilation Angle	Eccentricity	$f_{bo}/f_{co}$	K	Viscosity Parameter
35	0.1	1.16	0.667	0.004

### 3. Results and Discussions

#### 3.1. Introduction

This chapter presents research results on nonlinear finite element analysis for bare RC portal frames, strengthened with 0%-30% CFRP under cyclic loading, and three sub assemblages under gravity load inelastic finite element analysis. It evaluates seismic performance, failure mechanisms, and crack patterns for each frame, with discussions supported by graphs and tables.

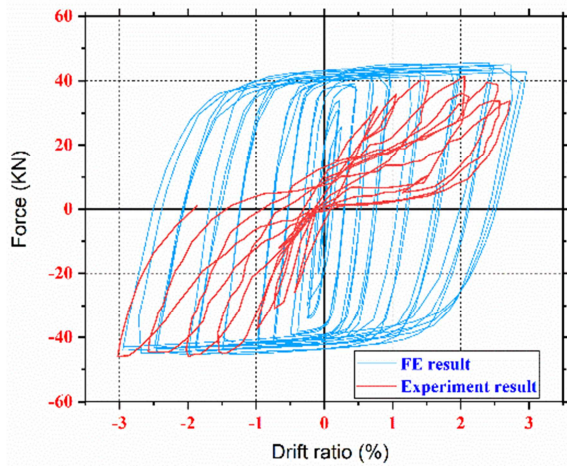


**Figure 13.** FEM and Experimental hysteretic load-drift ratio for RC frames.

#### 3.2. Validation of the Nonlinear Finite Element Model

##### 3.2.1. Validation of Finite Element Analysis Results

The behavior of the beam-column joint available in the literature was determined in the model. The data comprised of tests on the beam-column joint carried out by [13]. RC beam-column joint specimens subjected to displacement-controlled cyclic loading were tested. The geometric characteristics of the models and material properties are considered in the experimental work carried out by [13]. This was a reinforced concrete frame of columns with a cross-section of 300x350 mm and a height of 1365 mm and a cross-section of a beam of 300x350 mm and 2350 mm length. In all specimens, the beams and columns were reinforced with the top and bottom bars of 2Φ16 mm. In the columns, beam and beam-column joint, the steel stirrups consisted of 10 mm bars at 100 mm c / c spacing. The whole specimen will be fitted with a clear cover of 25 mm.

The comparative findings of the study carried by [13] and the numerical analysis finding achieved from finite element model carried out in this study. Figure 13 shows the difference in hysteretic curves in the finite element model and experimental specimens. The maximum lateral load of FEM and experimental curves is found to be 45.6 kN and 42.9 kN respectively. The finite element analysis and experimental findings obtained have 5.6% variation.

The first yield load of FEM and experimental curves is found to be 40.9 kN and 41.3 kN respectively. This shows that there is no significant difference between finite element analysis result and experimental results.

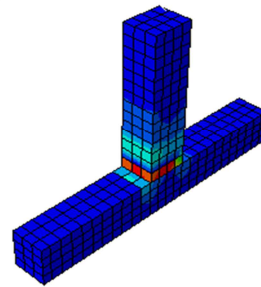
##### 3.2.2. Failure Patterns

The comparison of cracking pattern in the two specimens obtained by the FEA and reported from the experimental test results are discussed as the following.



PE, Max. Principal  
(Avg: 75%)

+1.88e-02  
+1.73e-02  
+1.57e-02  
+1.41e-02  
+1.26e-02  
+1.10e-02  
+9.42e-03  
+7.85e-03  
+6.28e-03  
+4.71e-03  
+3.14e-03  
+1.57e-03  
+0.00e+00



Max: +1.88e-02  
Elem: COLUMN-1.15  
Node: 92

Min: +0.00e+00  
Elem: BEAM-1.1  
Node: 175

Step: Loading Step  
Increment 71: Step Time = 2.371  
Primary Var: PE, Max. Principal



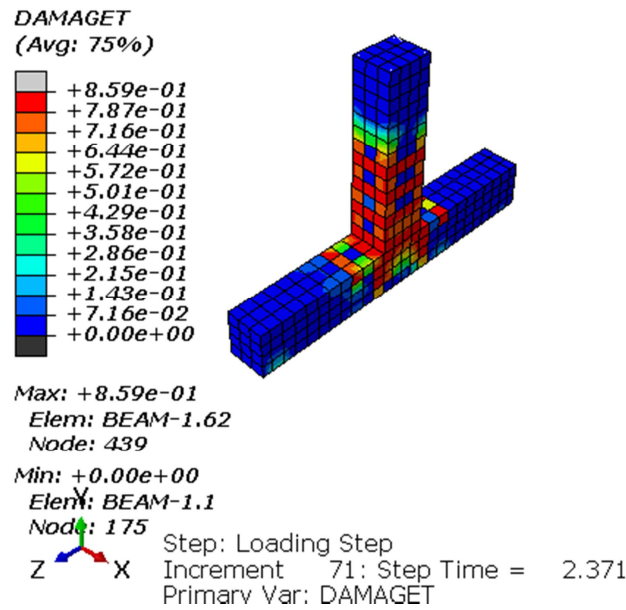


Figure 14. Comparison of crack patterns at maximum load.

The numerical model accurately predicts specimen failure, with cracking patterns consistent with experimental results. The predicted pattern is concentrated on the beam-column joint panel zone, confirming the model's strong capability in predicting specimen failure.

### 3.3. Finite Element Analysis Results and Discussions

In elastic finite element analysis results and discussions of for six first scheme RC portal frames (one bare RC frame and five RC frames strengthened with CFRP) and the second part were discussed in this sub-section of the thesis in terms of force-displacement curves, ultimate loads and displacements and cracking patterns.

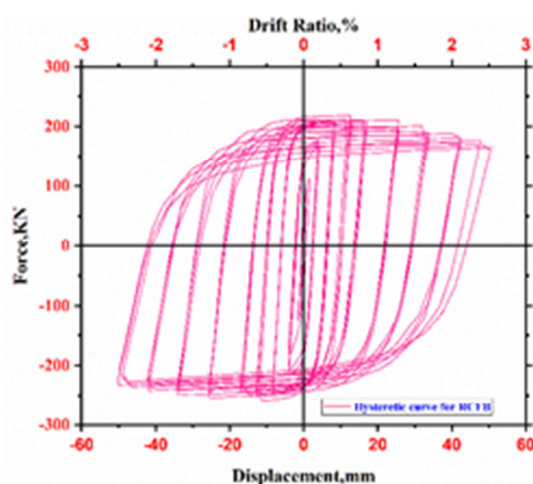
#### 3.3.1. Hysteretic Behavior of RC Portal Frames

This section analyzes RC frames' hysteretic behavior in terms of load-drift ratio, revealing that the frames reach their

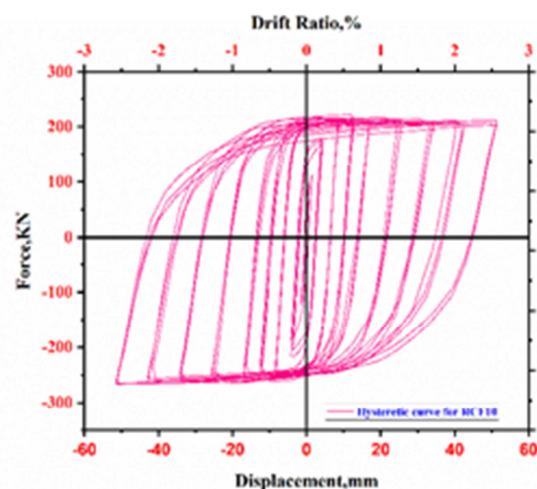
yield drift when they enter plastic phase, followed by concrete crushing and successive reinforcement bars yielding [12].

#### (i). Hysteretic Behavior for the First Schemes RC Frames

The bare frame 'RCFB' failed at load of 139.38KN with displacement of 3.62mm and the model with 10% CFRP 'RCF10' failed at 186.50KN with displacement 7.203mm. The other models RCF 15, RCF20, RCF20, RCF25 and RCF30 get collapsed at lateral load of 199.89KN, 202.04KN, 212.5KN and 230.45KN with lateral displacement 8.232mm, 7.889mm, 7.72mm and 7.37mm respectively. Comparing a 'RCFB' lateral load capacity with load capacity of other models, RCF10, RCF15, RCF20, RCF25 and RCF30 are 25.28%,30.27%,31%,34.24% and 39.52% respectively. The highest lateral load capacity in RCF30% achieved when compared to others frames.



(a)



(b)

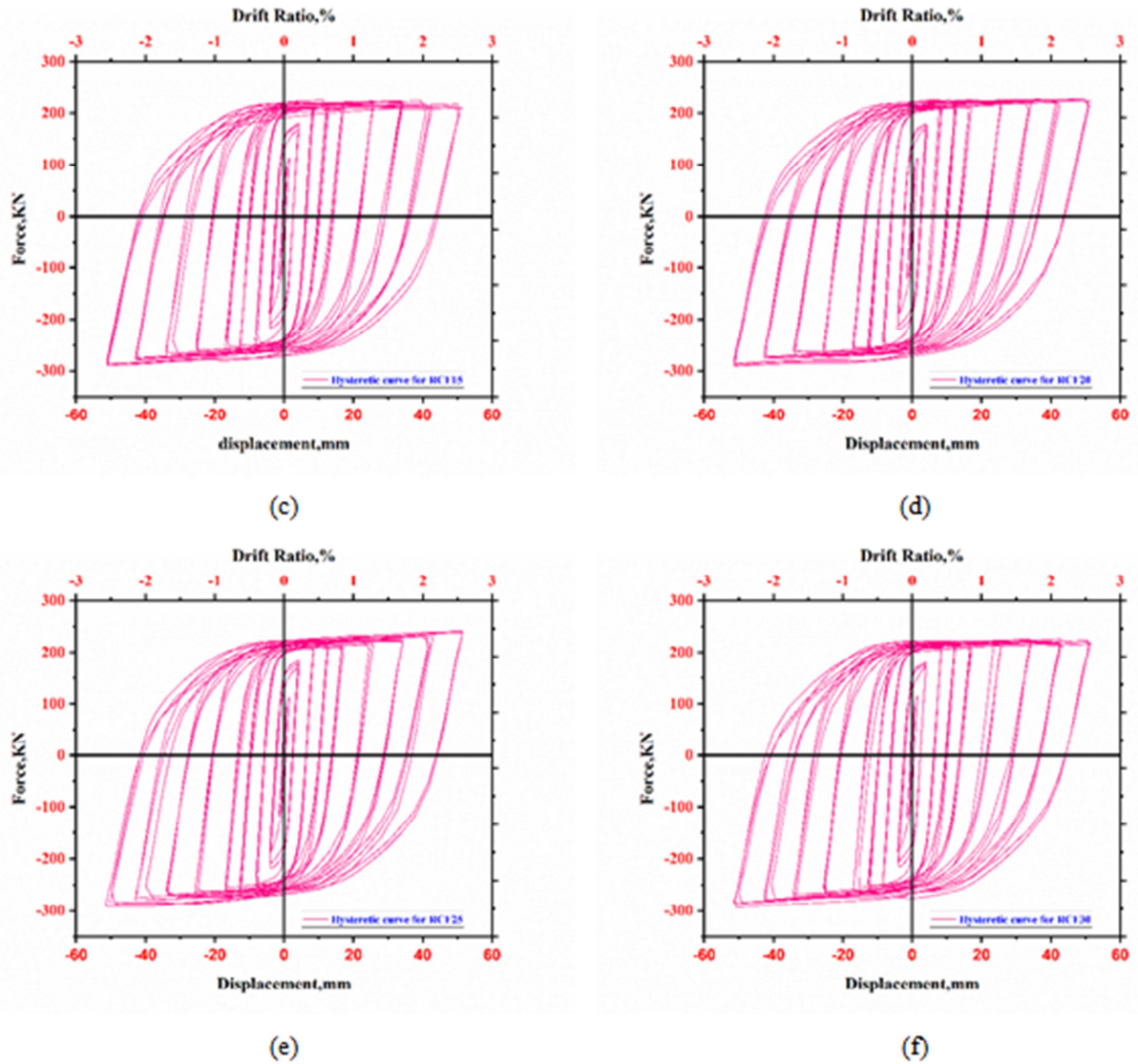
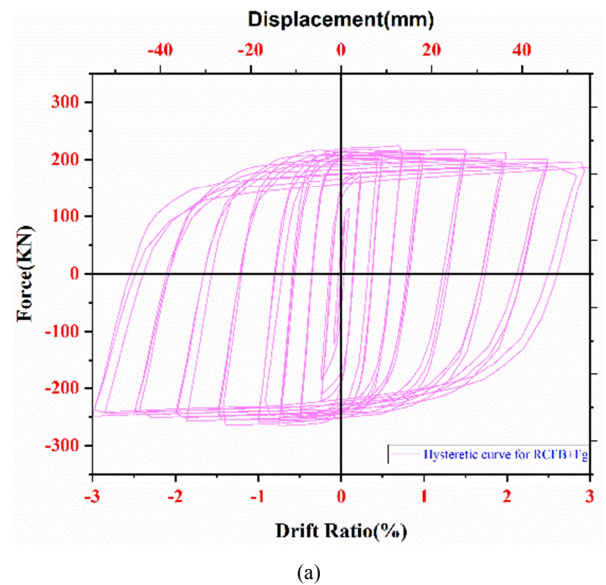


Figure 15. Hysteretic loops for the first schemes RC frames. (a) RCFB, (b) RCF10, (c) RCF15, (d) RCF20, (e) RCF25, (f) RCF30.

### (ii). Hysteretic Behavior for the Second Schemes RC Frames

In this sub section the effects of gravity load on the hysteretic behavior of RC frames subjected to cyclic loading were discussed. The bare frame 'RCFB+Fg' failed at load of 224.30KN with displacement of 11.9487mm and the model with 10% CFRP 'RCF10+Fg' failed at 228.79 KN with displacement 9.367mm. The other model RCF10+Fg which was strengthened with additional 10% of length of column with CFRP sheets near to the fixed support get collapsed at lateral load of 247.86 with lateral displacement 33.53 mm. Comparing a 'RCFB+Fg' lateral load capacity with load capacity of other two models, RCF10 +Fg and RCF10+Fg with additional CFRP sheets at the fixed support are 1.96% and 9.5% respectively. The highest lateral load capacity which is 247.86KN in RCF10+Fg with additional CFRP sheets near to fixed supports achieved when compared to others two frames.





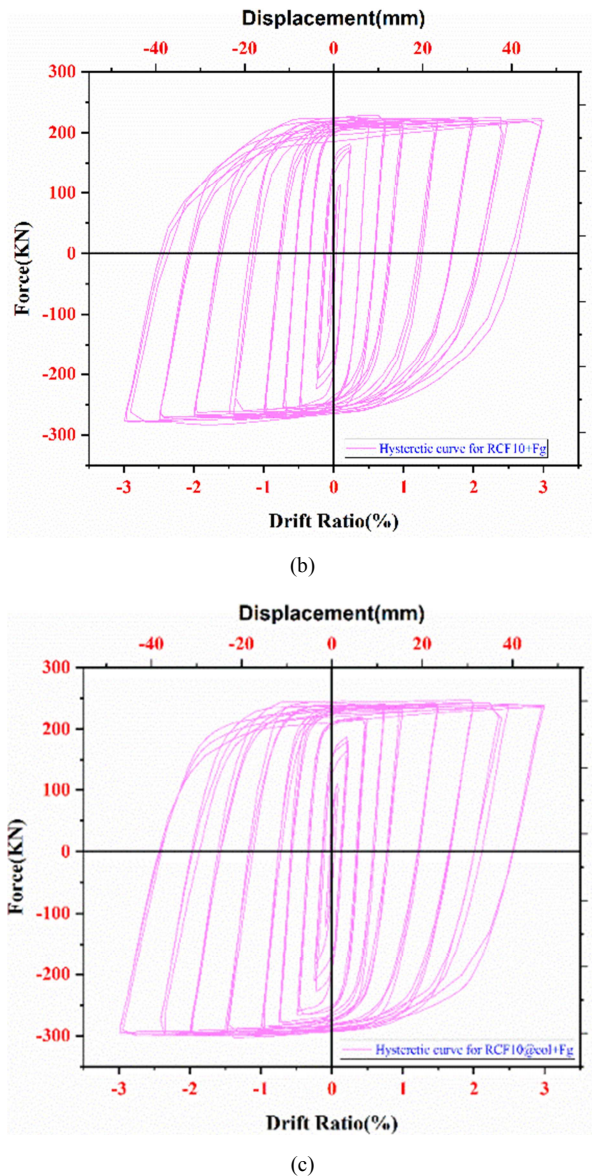


**Figure 16.** Hysteretic loops for the first schemes RC frames (a) RCFB+Fg, (b) RCF10+Fg, (c) RCF10+Fg with additional CFRP sheets near the supports.

Comparing the seismic performance of RCFB and RCFB+Fg the frame with gravity load shows 2.67% lateral load capacity than the RCFB and also RCF10+Fg shows 3.10% lateral load capacity than RCF10 which subjected to lateral load only. Comparing a 'RCF10+Fg with additional CFRP sheets near to the fixed support of frame' lateral load capacity with load capacity of other models, RCF10, RCF15, RCF20 and RCF25 11.83%, 10.55%, 8.95%, 8.23% and 2.74% respectively. The highest lateral load capacity in RCF10+Fg additional CFRP sheets near to the fixed support of frame achieved when compared to others frames of the first schemes.

### 3.3.2. Envelope Curves for RC Portal Frames

A cyclic envelope curve is a force-displacement curve that envelopes the hysteretic behavior of a component or assembly that is subjected to cyclic loading. The following

subsection of this chapter shows the envelope curves for all six RC frames of the first schemes and all three RC frames of the second schemes.

#### (i). Envelope Curves for First Schemes

Figure 17 shows a cyclic envelope of all six RC frames of the first schemes, which is defined by connecting the peak force responses at each displacement level and shows the relationship between the peak loads at every cycle and the respective drift ratio. As shown in the figure the maximum load carrying capacity of RC frames increase slightly as CFRP percentage increase bare RCFB to RCF30.

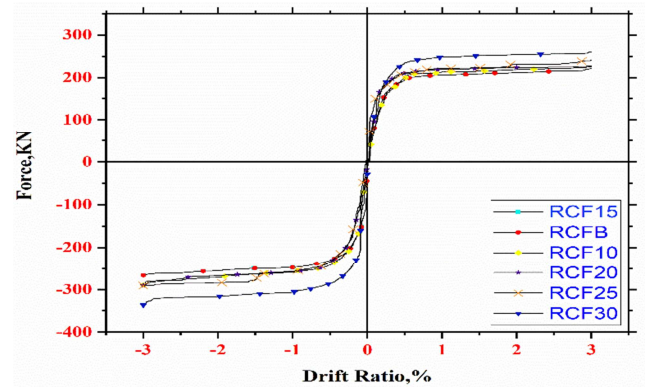


**Figure 17.** Envelope curves for all first schemes RC frames.

#### (ii). Envelope curves for the second Schemes Frames

Figure 18 shows a cyclic envelope of all three RC frames for second schemes frames, which is defined by connecting the peak force responses at each displacement level and shows the relationship between the peak loads at every cycle and the respective drift ratio. As shown in the figure the maximum load carrying capacity of RC frames increase slightly as CFRP percentage increase bare RCFB+Fg to RCF10+Fg with additional CFRP sheets near the supports.

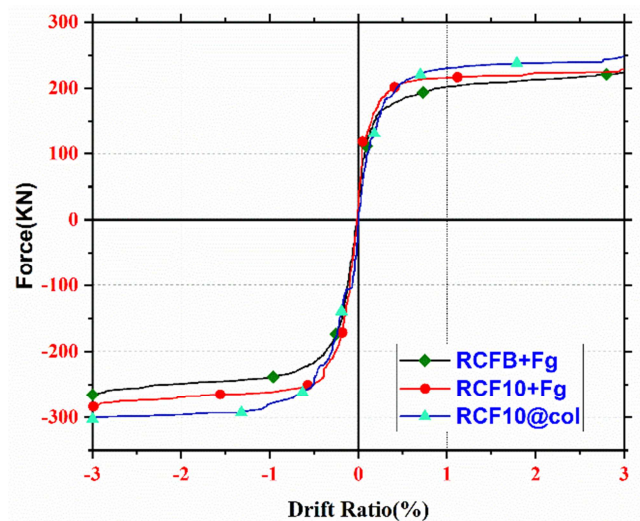


**Figure 18.** Envelope curves for all first schemes RC frames.

### 3.3.3. Damage and Failure Pattern

The CDP model indicates cracking initiation and

propagation through maximum principal plastic strain. It simulates nonlinear behavior of quasi-brittle materials in tension and compression. Damage and cracking behavior are expressed in output parameters, including concrete tensile, compressive, joint shear stress, reinforcement Von-Mises stress, and maximum principal plastic strain cracking pattern.

#### (i). Damage Patterns for First Schemes RC Frames

##### *Bare Reinforced concrete frame RCFB Model*

The bare reinforced concrete frame modeled with reinforced concrete without any carbon fiber. Figure 19-21 illustrates the damage progress and developed crack patterns during the simulation at different drift ratio of the Bare

Reinforced concrete frame (RCFB).

When the frame was loaded, the initial flexural cracks are observed during the first positive loading cycle of 0.12% drift ratio at the bottom of the column and at beam near to the column joints. The specimen continued to exhibit more flexural cracks during the last cycle at 0.12 % drift ratio. While increasing the loading cycles, more flexural cracks are initiated and gradually upgraded into the full depth of the beam plastic hinge zone. Figure 19 illustrates the tensile damage and maximum principal plastic strain cracks of this specimen after completing the first three cycles of 0.12% drift ratio.

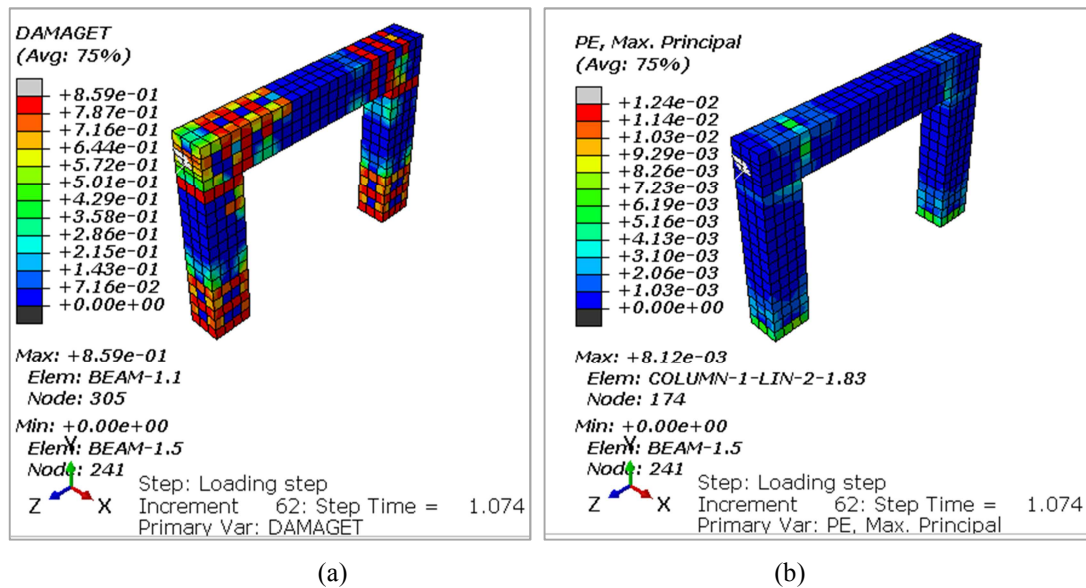
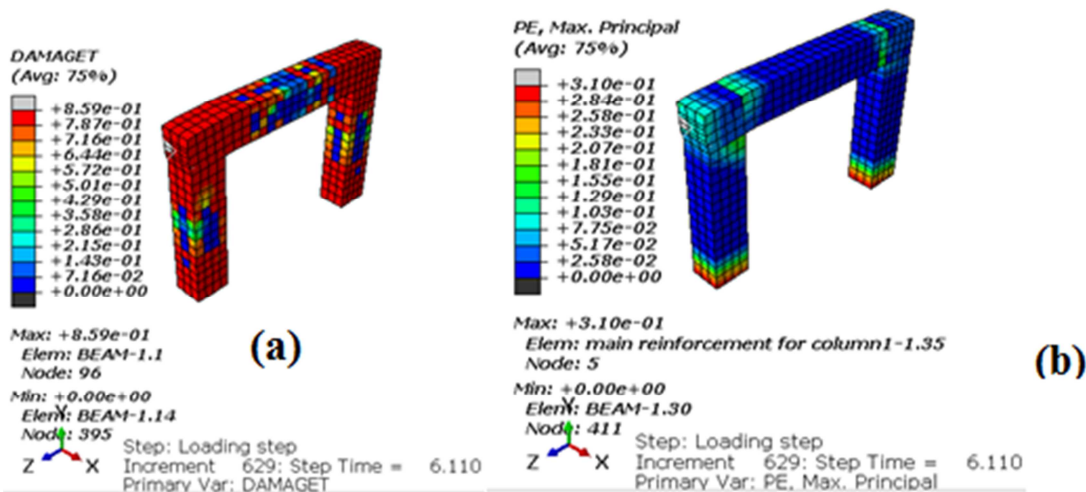


Figure 19. Observed failure patterns of RCFB after completing 0.12 % drift ratio. (a) Concrete tensile damage, (b) Maximum principal plastic strain cracks

Up to of 0.20% drift ratio, cracks can be identified as flexural crack. When a loading cycle reached at the first cycle of 0.25% drift ratio, minor diagonal cracks initiated to the beam column joint panel zone. With continuing of loading, a significant concrete tensile damage displayed, the significant dense cracks forming in the joint region and

significant palling of concrete compression damage occurred at the last cycle of 0.5% drift ratio as depicted in Figure 20. Moreover, the beam and columns stirrups bars were exposed to tensile stress and initiated to yielding at this stage of loading [see Figure 20 (d)].





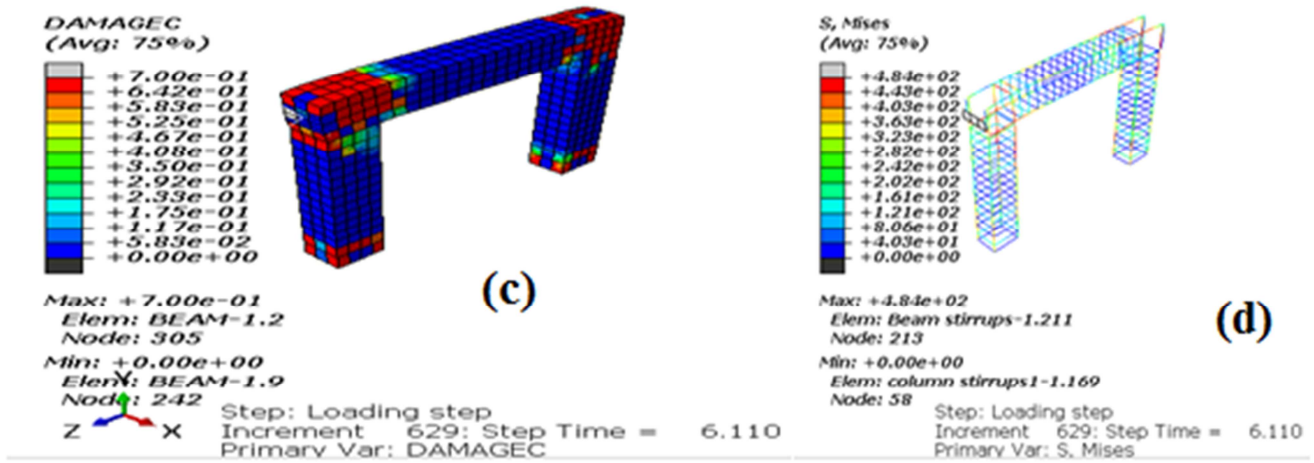


Figure 20. Observed damage and failure patterns of RCFB at 1.38% drift ratio. (a) Concrete tensile damage, (b) Maximum principal plastic strain cracks, (c) Concrete compressive damage, (d) Reinforcement Mises stress.

With further increasing of loading cycles, the cracks significantly accumulate and widen in the joints as well as in the beam and columns and the RCFB had lost more and more of its maximum load-carrying capacity. The damage and failure patterns in the third cycle of the 3% drift ratio the maximum loading step as shown in Figure 21. As observed

from the failure mode, the failure of the joints zones comes first before failures of beam. Significant deformation of the beam and columns were followed by the occurrence of the plastic hinge at the beam-column junction. Therefore, the final failure of the bare RC frame is identified as a combination of beam and joint failure (B-J failure).

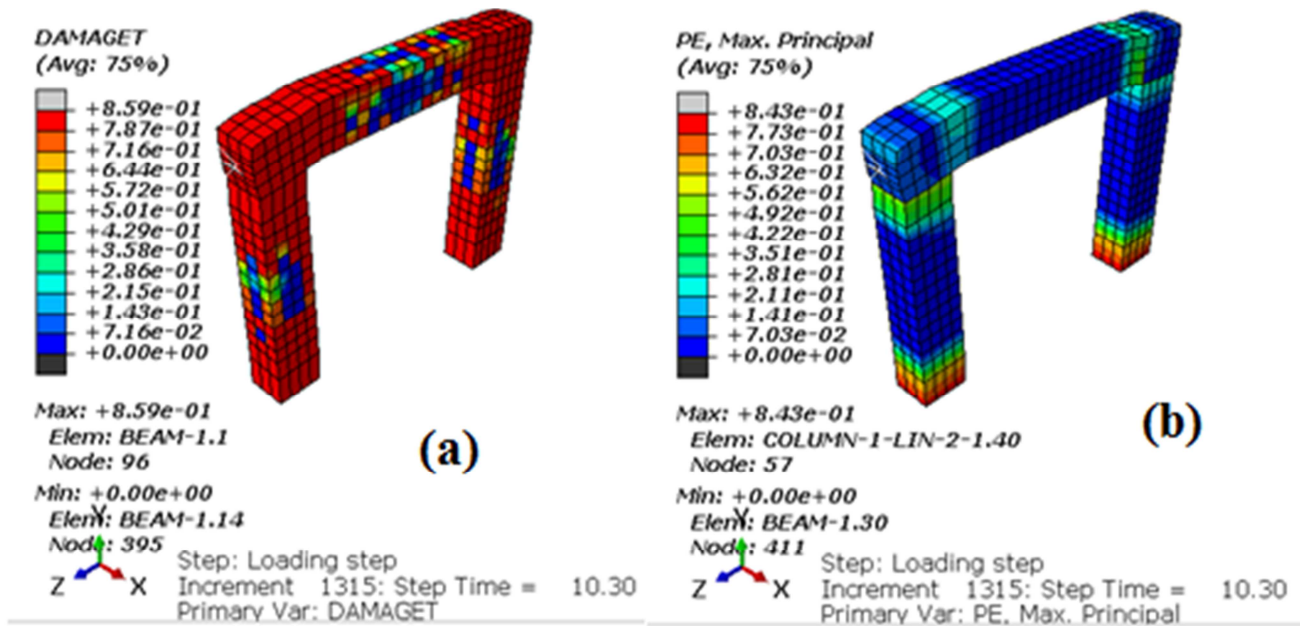


Figure 21. Observed damage and failure patterns of RCFB at 3 % drift ratio. (a) Concrete compressive damage, (b) Maximum principal plastic strain cracks

#### RCF10

The RC frame strengthened with 10% of CFRP has similar materials properties and reinforcement details as RCFB. The only difference is RCF10 is strengthened with 10% CFRP around the beam column joints in which crack failure is large in the first model.

Figure 22-23 shows the damage progression and developed crack patterns during the simulation at different

loading stages of the specimen RCF10. The initial flexural cracks in RCF10 model is induced near to the beam-column joint and at the bottom of column at the first cycle of 0.16% drift ratio. However, unlike the RCFB, no further damage was observed during the first few cycles in this specimen. This is due to the strengthening with 10% CFRP Figure 22 shows specimen RCF10 after completing the three cycles of 0.16% drift ratio.



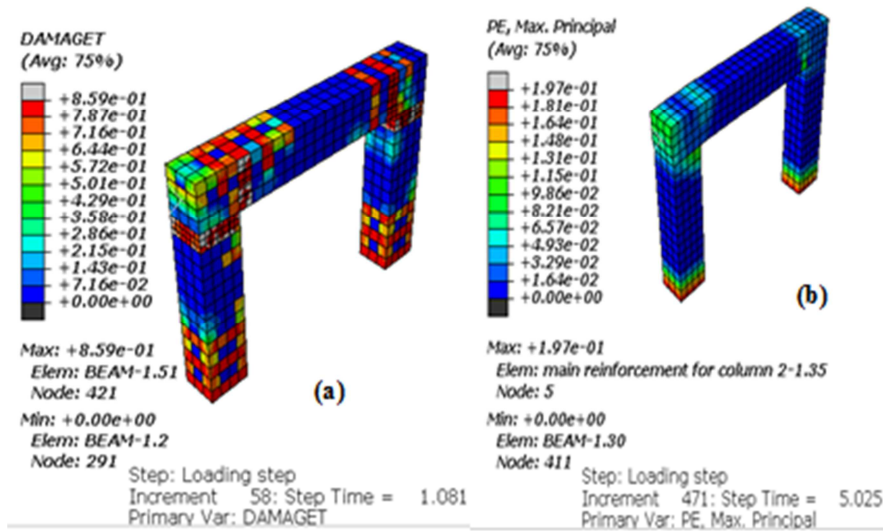


Figure 22. Failure patterns of RCF10 after three cycles at 0.16% drift ratio. (a) Concrete tensile damage (b) Maximum principal plastic strain.

The following figures show damage progression and developed crack patterns of RCF10 at 1.38 drift ratio. As shown in figure damage intensity and crack patterns of

RCF10 are slow when we compare with the CFPB. There is no significant difference of flexural cracks when compared with the RCFB model.

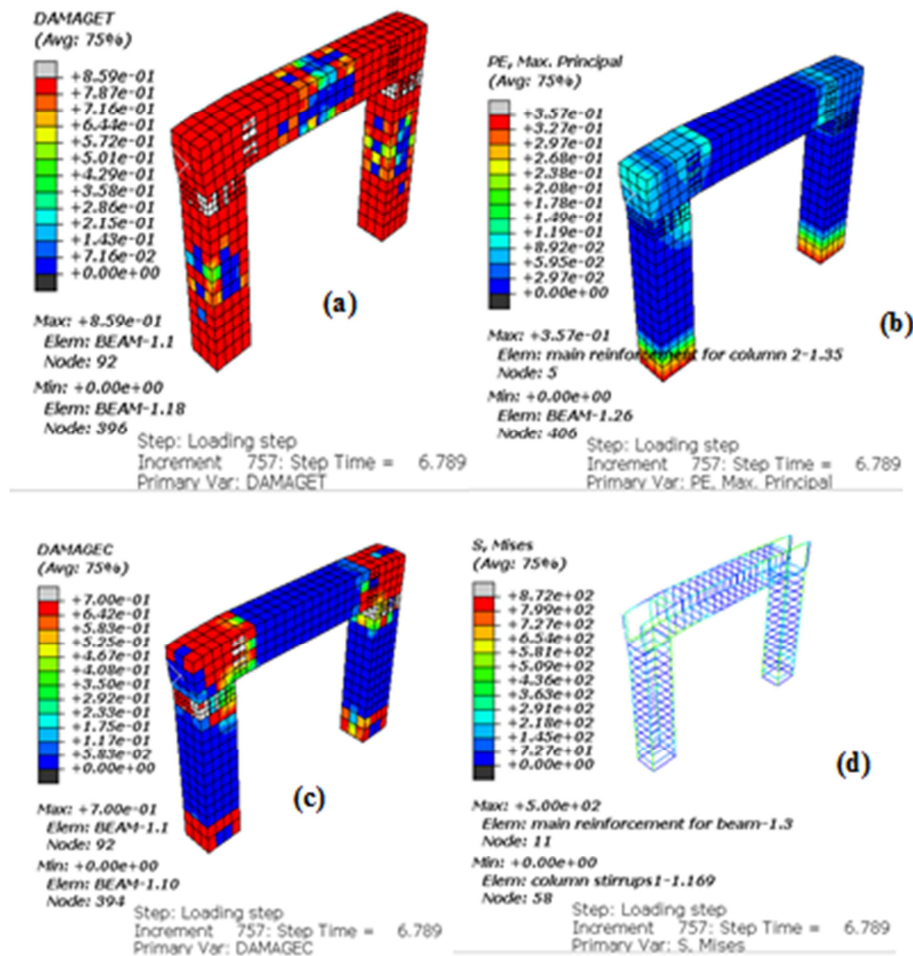


Figure 23. Observed damage and failure patterns of RCF10 at 1.38% drift ratio. (a) Concrete tensile damage, (b) Maximum principal plastic strain, (c) Concrete compressive damage, (d) Reinforcement Mises stress.

As the hysteretic loops of the force-drift ratio of all models show there is a little increase of load resistance capacity of

the frames under seismic loading. Generally, the ultimate loading capacity for each RC frame was reached its

maximum at less than 0.5% drift ratio for all frames with insignificant differences between them.

## (ii). Damage Patterns for the Second Schemes RC Frames

### Bare Reinforced concrete frame (RCFB+Fg) Model

The bare reinforced concrete frame modeled with reinforced concrete without any carbon fiber subjected to lateral cyclic loading and gravity load on beam critical section. Figure 24-25 illustrates the damage progress and developed crack patterns during the simulation at different drift ratio of the Bare Reinforced concrete frame (RCFB+Fg) of the second schemes of RC portal frames.

When the frame was loaded, the initial cracks are observed during the last positive loading cycle of 0.2% drift ratio at the bottom of the columns. The specimen continued to exhibit more flexural cracks during the last negative cycle at 0.2 % drift ratio. While increasing the loading cycles, more flexural cracks are initiated and gradually upgraded into the full depth of the beam plastic hinge zone. Figure 24 illustrates the tensile damage and maximum principal plastic strain cracks of this specimen after completing the first three cycles of 0.25% drift ratio.

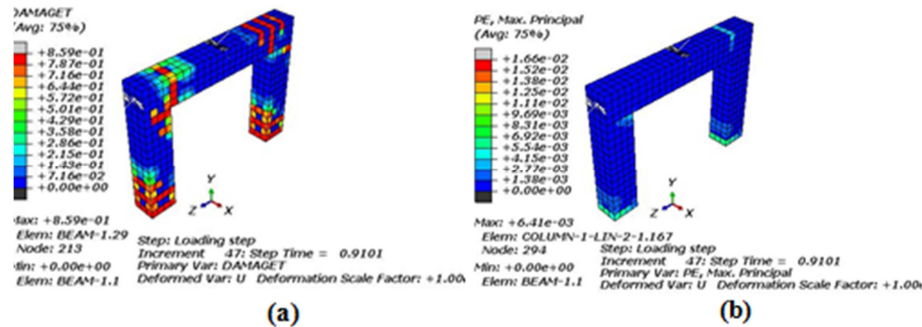


**Figure 24.** Observed failure patterns of RCFB+Fg after completing 0.25% drift ratio. (a) Concrete tensile damage, (b) Maximum principal plastic strain cracks

With further increasing of loading cycles, the cracks significantly accumulate and widen in the joints as well as in the beam and columns and the RCFB+Fg had lost more and more of its maximum load-carrying capacity. The damage and failure patterns in the third cycle of the 0.5% drift ratio the maximum loading step as shown in Figure 25 As observed

from the failure mode, the failure of the joints zones comes first before failures of beam. Significant deformation of the beam and columns were followed by the occurrence of the plastic hinge at the beam-column junction. Therefore, the final failure of the bare RC frame is identified as a combination of beam and joint failure.

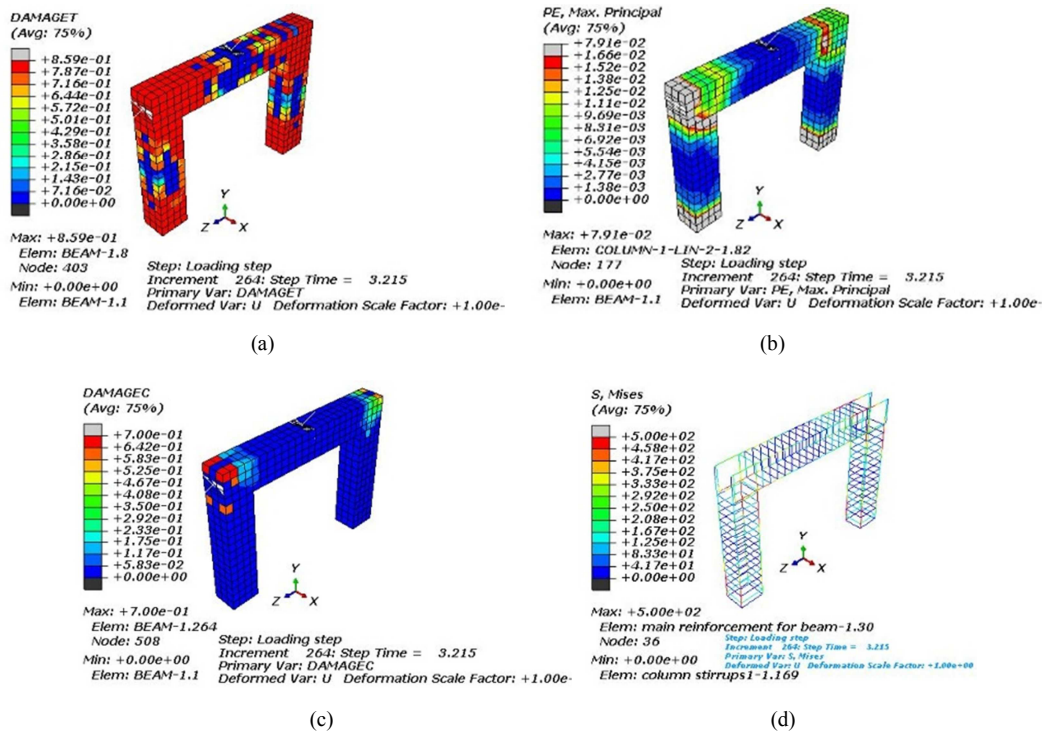


**Figure 25.** Observed damage and failure patterns of RCFB+Fg at 0.5% drift ratio. (a) Concrete tensile damage, (b) Maximum principal plastic strain, (c) Concrete compressive damage, (d) Reinforcement Mises stress.

## RCF10+Fg Model

The RC frame strengthened with 10% of CFRP has similar materials properties and reinforcement details as RCFB. The only difference is RCF10+Fg is strengthened with 10% CFRP around the beam column joints in which crack failure is large in the first model and subjected to gravity load on the beam critical zones.

When the frame was loaded, the initial cracks are observed during the first positive loading cycle of 0.1% drift ratio at

the bottom of the columns. The specimen continued to exhibit more flexural cracks during the last negative cycle at 0.1 % drift ratio. While increasing the loading cycles, more flexural cracks are initiated and gradually upgraded into the full depth of the beam plastic hinge zone. Figure 26 illustrates the tensile damage and maximum principal plastic strain cracks of this specimen after completing the first three cycles of 0.1% drift ratio.

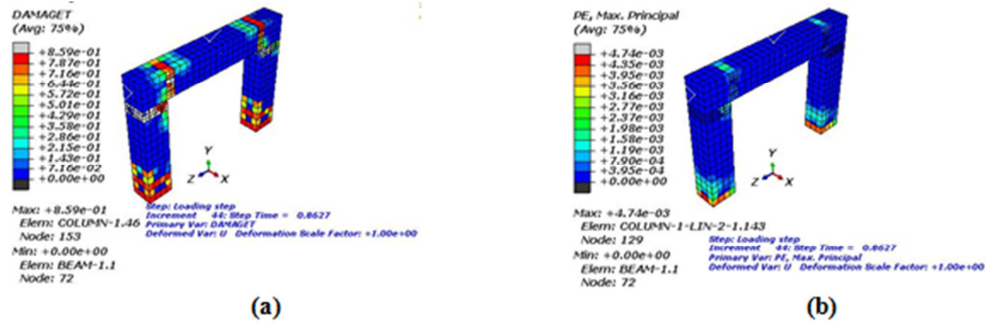


Figure 26. Observed failure patterns of RCF10+Fg after completing 0.1% drift ratio. (a) Concrete tensile damage, (b) Maximum principal plastic strain cracks.

With further increasing of loading cycles, the cracks significantly accumulate and widen in the joints as well as in the beam and columns and the RCF10+Fg had lost more and more of its maximum load-carrying capacity. The damage and failure patterns in the third cycle of the 0.5% drift ratio the maximum loading step as shown in Figure 27. As observed

from the failure mode, the failure of the joints zones comes first before failures of beam. Significant deformation of the beam and columns were followed by the occurrence of the plastic hinge at the beam-column junction. Therefore, the final failure of the RCF10+Fg frame is identified as a combination of beam and joint failure.

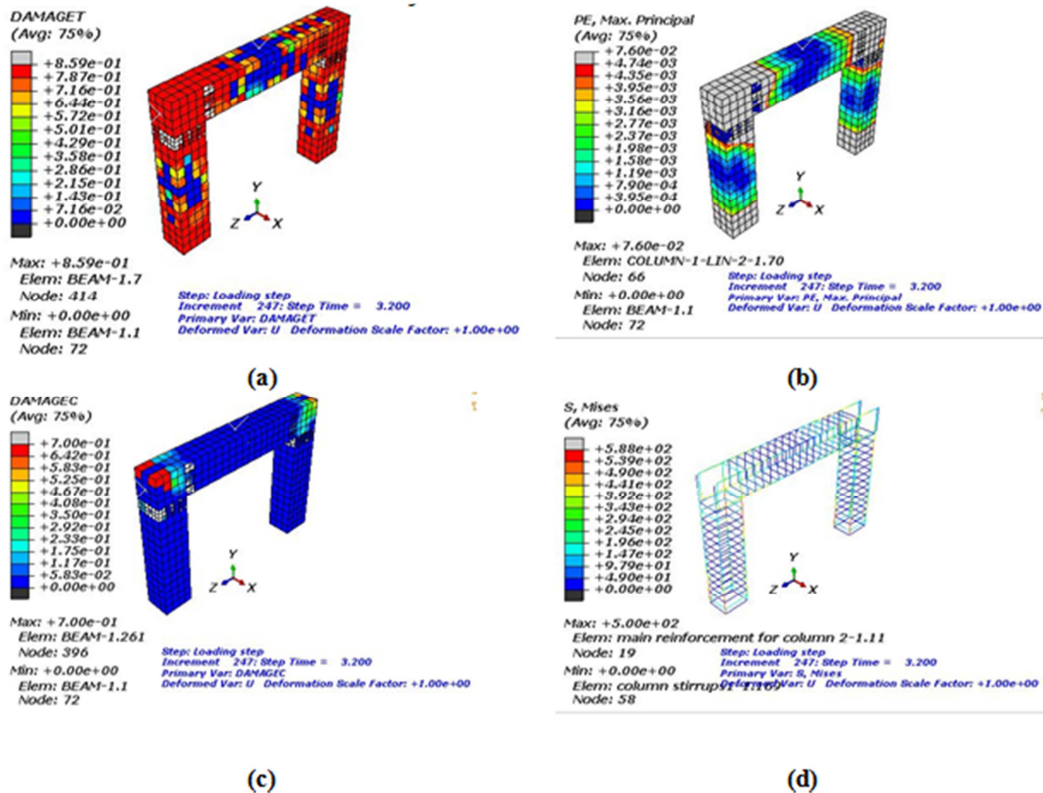


Figure 27. Observed damage and failure patterns of RCF10+Fg at 0.5% drift ratio. (a) Concrete tensile damage, (b) Maximum principal plastic strain, (c) Concrete compressive damage, (d) Reinforcement Misses stress.



RCF10+Fg with additional CFRP sheets near to Fixed supports Model

The RCF10+Fg modeled with reinforced concrete with CFRP sheets near to the beam-column joints on the beam and columns, and near to the fixed support on the bottom sections of columns subjected to lateral cyclic loading and gravity load on beam critical section. Figure 28-29 illustrates the damage progress and developed crack patterns during the simulation at different drift ratio of the Bare Reinforced concrete frame (RCF10+Fg) of the second schemes of RC portal frames.

When the frame was loaded, the initial cracks are observed during the last positive loading cycle of 0.25% drift ratio at the bottom of the columns. The specimen continued to exhibit more flexural cracks during the last negative cycle at 0.25% drift ratio. While increasing the loading cycles, more flexural cracks are initiated and gradually upgraded into the full depth of the beam plastic hinge zone. Figure 28 illustrates the tensile damage and maximum principal plastic strain cracks of this specimen after completing the first three cycles of 0.25% drift ratio.

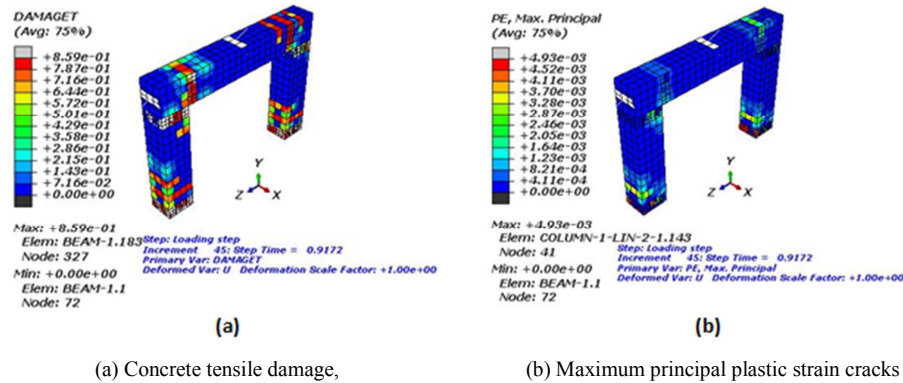


Figure 28. Observed failure patterns of RCF10+Fg with additional CFRP sheets near to Fixed supports Model after completing 0.25% drift ratio.

With further increasing of loading cycles, the cracks significantly accumulate and widen in the joints as well as in the beam and columns and the frame had lost more and more of its maximum load-carrying capacity. The damage and failure patterns in the third cycle of the 1.5% drift ratio the maximum loading step as shown in Figure 29. As observed

from the failure mode, the failure of the joints zones comes first before failures of beam. Significant deformation of the beam and columns were followed by the occurrence of the plastic hinge at the beam-column junction. Therefore, the final failure of the bare RC frame is identified as a combination of beam and joint failure.

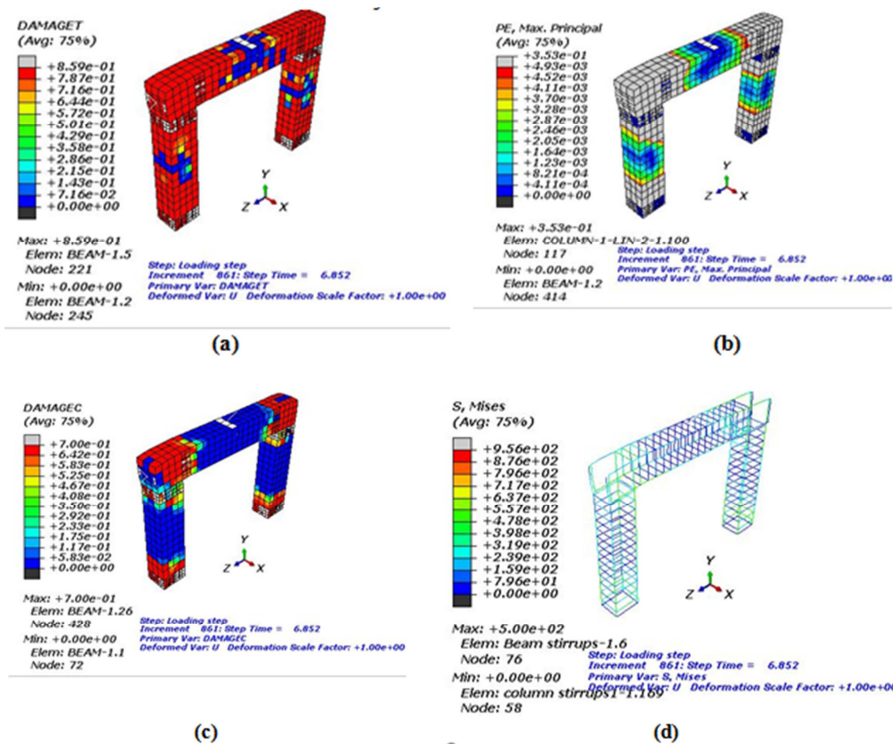


Figure 29. Observed damage and failure patterns of RCF10+Fg at 1.5 % drift ratio. (a) Concrete tensile damage, (b) Maximum principal plastic strain, (c) Concrete compressive damage, (d) Reinforcement Misses stress.

### 3.3.4. Energy Dissipation Capacity

The ability to disperse inelastic deformation energy is a key factor that can be used to evaluate the performance of the RC frames for which seismic action has been carried out. The energy distributed by the specimen within an individual cycle,  $E_i = \int P_i d\Delta$ , was described as the area covered by the load-displacement hysteresis loop. It was then found that the total energy dissipated was the aggregate of the total energy dissipated in each simulated model cycle. When the displacement level increases, there is an increase in the energy dissipated in each cycle.

Energy dissipation Capacity of first scheme RC Frames

The dissipation energy of RC frame increased from 2.39%-7.39% for 10% CFRP strengthened frame to 30% CFRP strengthened frame. Generally, the dissipated energy of most models showed the same trend not significant difference was observed.

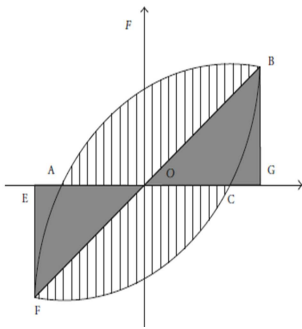


Figure 30. The dissipation capacity area.

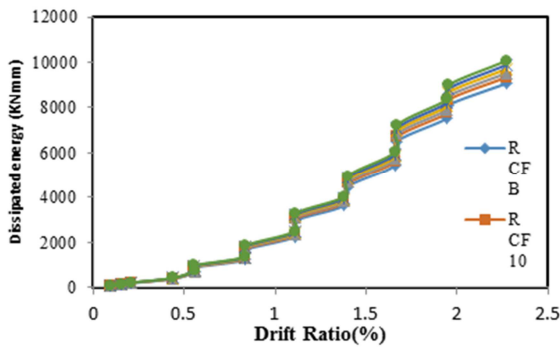


Figure 31. Comparison of the energy dissipated in the first cycle of each drift ratio.

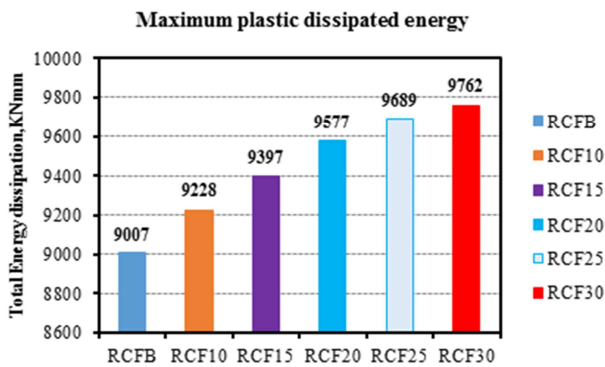


Figure 32. Maximum plastic dissipated energy for the six frames.

Table 6. Maximum dissipation energy and their percentages of increasing.

Frame	Energy Dissipation (KN.mm)	
	Area	Increasing (%)
RCFB	9007	0
RCF10	9228	2.39
RCF15	9397	4.15
RCF20	9577	5.95
RCF25	9689	7.04
RCF30	9762	7.39

Energy dissipation Capacity of the Second scheme RC Frames

Negative deformation in portal frame systems under cyclic loads leads to unidirectional plastic hinges. To improve energy dissipation, increase beam critical region resistance over ductility. The dissipation energy of the second schemes of RC frame increased by 3.58% and 3.37% for 'RCFB+Fg' and 'RCF10+Fg' comparing to RCFB and RCF10 of the first schemes frames respectively.

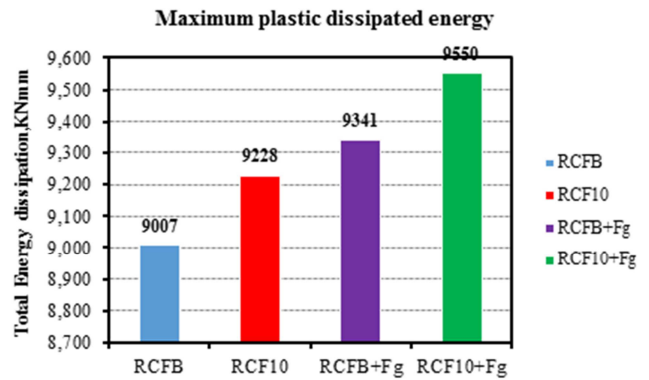


Figure 33. Maximum plastic dissipated energy for the four RC frames.

### 3.3.5. Ductility

A significant factor for earthquake resistant construction is ductility. To compare the ductility of the RC frames, the displacement ductility ratio  $\mu_\Delta$ , defined as the ratio of ultimate displacement  $\Delta_u$  to the yield displacement  $\Delta_y$  at the initial yield of internal steel or to the first crack. To facilitate the calculation of displacements ductility factor at the initial yield of steel or at the foremost crack, the average value of yield displacements, and ultimate displacement were adopted and factor can be calculated using equation...

$$\mu_\Delta = \frac{\bar{\Delta}_u}{\bar{\Delta}_y} = \frac{|\Delta_{u+}| + |\Delta_{u-}|}{|\Delta_{y+}| + |\Delta_{y-}|}$$

Where,  $\Delta_{u+}$  and  $\Delta_{u-}$  = positive and negative ultimate displacement respectively, and  $\Delta_{y+}$  and  $\Delta_{y-}$  = positive and negative yield displacement respectively.

The  $\Delta_y$  is attained according to the general yield moment method [45]. The displacement at the yielding is assumed as the abscissa of the intersection point of Line OB and the horizontal at the peak load in Figure 34. Point B on the load versus displacement curve has the same abscissa of Point A, which is the intersection point between the tangent line of the skeleton curve at original and the horizontal line of ultimate



load.

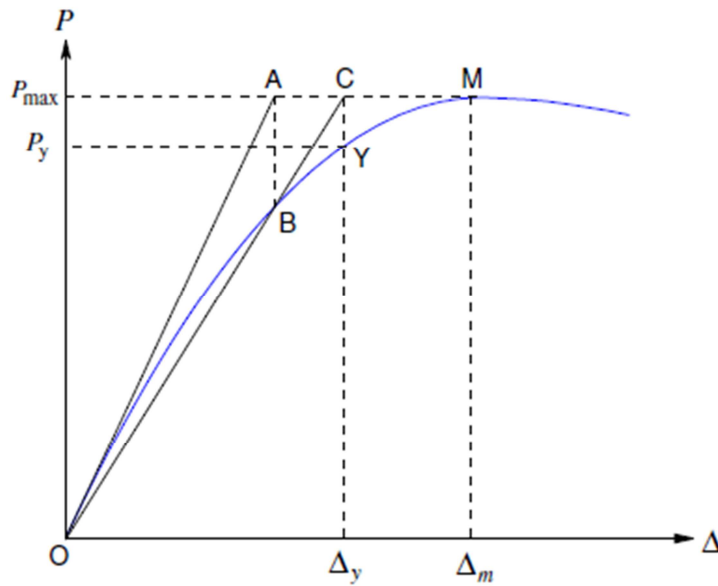


Figure 34. General Yield moment method diagram (Zhu, 1989).

Table 7. The displacement ductility factor for each RC frames.

RC Frames	Yield displacement $\Delta_y$ (mm)		Ultimate displacement $\Delta_u$ (mm)		Displacement ductility factor ( $\mu$ )		Average ductility factor ( $\mu$ )	Percentage of increased
	Positive	negative	Positive	negative	Positive	negative		
RCFB	1.715	3.087	2.915	3.94	1.7	1.28	1.49	-
RCF10	3.78	3.82	7.03	7.62	1.9	2	1.95	24
RCF15	4.11	3.78	6.35	12.52	1.54	3.31	2.43	38.67
RCF20	4.29	4.06	6.86	13.89	1.6	3.42	2.51	40.63
RCF25	4.63	5.49	7.89	25.55	1.7	4.65	3.18	53.14
RCF30	5.15	5.74	9.947	25.73	1.93	4.48	3.21	53.58

It can be seen that there is an increase in ductility of the strengthened frames with 30% of CFRP by almost 53.58% in comparison to the bare frame.

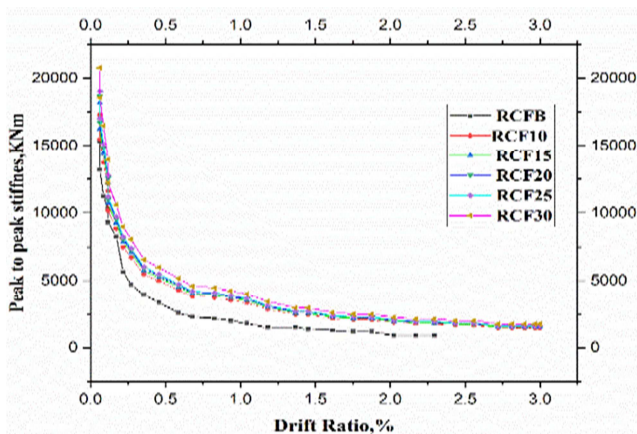


Figure 35. Comparison of the peak-to-peak stiffness at each drift ratio for the six models.

### 3.3.6. Stiffness Degradation

Structural resistance to seismic load is determined by the loss of stiffness across loading cycles, with increased stiffness loss occurring at different rates. Peak displacement is represented by decreased slopes of load-displacement

hysteresis loops. Figure 35 reveals that the bare frame (RCFB) initially has higher stiffness than the CFRP retrofitted frames. However, with increased lateral sway, all models lose stiffness. The stiffness decreases due to beam-column joint cracks after a drift ratio of 0.5%. The strengthened frames show greater stiffness throughout the FEA, but no significant change is observed.

## 4. Conclusions and Recommendations

### 4.1. Conclusions

This chapter provides an overview of a finite element investigation on the performance of reinforced concrete frames under displacement controlled cyclic loading, examining the impact of gravity loads on hysteretic behavior and the effects of strengthening with carbon fiber reinforced polymer on seismic behavior.

1. It is evident that strengthening RC frames with CFRP improved the behavior compared to that of the bare RC frame in terms of strength, total energy dissipated, energy dissipated as a function of a single cycle undergone for a certain drift ratio, as well as stiffness degradation. Base on cyclic loading analysis by ABAQUS, the hysteresis graph shows that the frames

with CFRP are slightly different from a bare frame. Energy Dissipation of CFRP strengthened frames is greater than the bare frame. The dissipation energy of RC frame increased from 2.39%-7.39% for 10% CFRP strengthened frame to 30% CFRP strengthened frame.

2. Even though the strengthened RC frame models have almost equal strength at first yielding with the bare RC frame the strengthened RC frames out-performed its counterpart in yielding strength and ultimate strength.
3. Carbon fiber helps delay visible crack initiation, reduces concrete spalling damages, and prevents joint shear failure by restraining crack widening and preserving beam-column joint concrete core integrity by changing failure modes.
4. The load-displacement response for all strengthened RC frame is flattened and then degraded slowly after yielding of internal steel due to localized debonding of the fiber and the bars.
5. The inclusion of gravity load effects in finite element analysis provides more realistic results than RC frame subjected to lateral cyclic loads. Strengthening the RC frame with additional CFRP sheets improves seismic performance. The highest lateral load capacity is achieved in RCF10+Fg additional CFRP sheets.

To summarize, this study proved the effectiveness of CFRP strengthening techniques in improving the performance of RC frames subjected to the cyclic loading.

#### 4.2. Recommendations for Future Work

The study highlights the need for further investigation into the behavior of RC portal frames, suggesting the use of one-layer CFRP for strengthening and double-layer CFRP for cyclic loading performance, and the use of CFRP as an internal reinforcement system.

## References

- [1] Aslani, H., and E. Miranda. 2005. "Probabilistic earthquake loss estimation and loss disaggregation in buildings." Ph. D. dissertation. Dept. of Civil and Environmental Engineering, Stanford Univ.
- [2] Abaqus Analysis User Manual – Abaqus Version 6.8. (2008). Retrieved November 5, 2010, from <http://bee-pg-031941:2080/v6.8/books/usb/default.htm>
- [3] Balamuralikrishnan, R., Al Madhani, M. and Al Madhani, R. "Study on Retrofitting of RC Column Using Ferrocement Full and Strip Wrapping." *Journal of Civil Engineering* 5(14) (November 2019): 2472-2485.
- [4] Behnam, H., Kuang, J. S. and Samali, B., 2018. Parametric finite element analysis of RC wide beam-column connections. *Computers & Structures*, 205, pp. 28-44.
- [5] Bento, R., Falcão, S., & Rodrigues, F. (2004). 13th World Conference on Earthquake Engineering Non-Linear Static Procedures in Performance Based Seismic Design, (2522).
- [6] Beydokhty EZ, Shariatmadar H (2016) Behavior of damaged exterior RC beam-column joints strengthened by CFRP composites. *Lat Am J Solids Struct* 13: 880–897.
- [7] Brena, S. F., and G. N. McGuirk. 2013. "Advances on the behavior characterization of FRP-anchored carbon fiber-reinforced polymer (CFRP) sheets used to strengthen concrete elements." *Int. J. Concr. Struct. Mater.* 7 (1): 3–16.
- [8] Birtel V, Mark P. Parameterised finite element modelling of RC beam shear failure. In: ABAQUS users' conference; 2006. p. 95–108.
- [9] Celik, O. C., and B. R. Ellingwood. 2010. "Seismic fragilities for nonductile reinforced concrete frames—Role of aleatoric and epistemic uncertainties." *Struct. Saf.* 32 (1): 1–12.
- [10] Chen, W. F., & Lui, E. M. (2006). *Earthquake Engineering for Structural Design*. London, New York.
- [11] Dan S, Bob C, Badea C, Dan D, Florescu C, Cotoarba L, Gruin A (2018) Carbon fiber reinforced polymers used for strengthening of existing reinforced concrete structures. *Mater Plast* 55(January): 536–540.
- [12] Dalalbashi, A., Eslami, A., and Ronagh, H. R. (2013). "Numerical investigation on the hysteretic behavior of RC joints retrofitted with different CFRP configurations." *Journal of Composites for Construction*, 17(3), 371-382.
- [13] Elias I. Saqan, Hayder A. Rasheed. And T. Alkhrdaji. "Evaluation of the seismic performance of reinforced concrete frames strengthened with CFRP fabric and NSM bars". *Composite Structures* 184 (2018) 839–847.
- [14] Eslami, A., Dalalbashi, A., and Ronagh, H. R. (2013). "On the effect of plastic hinge relocation in RC buildings using CFRP." *Compos Part B-Eng*, 52(0), 350-361.
- [15] Dowrick, D. (2009). *Earthquake Resistant Design and Risk Reduction (Second Edi)*. Tauranga, New Zealand.
- [16] Fajfar, P., & Eeri, M. (2000). *A Nonlinear Analysis Method for Performance Based Seismic Design*, 16(3), 573–592.
- [17] Federal Emergency Management Agency [FEMA]. (2000). *Prestandard and Commentary for the Seismic Rehabilitation of Buildings*. Washington, USA.
- [18] Goulet, C. A., C. B. Haselton, J. Mitrani-Reiser, J. L. Beck, G. G. Deierlein, K. A. Porter, and J. P. Stewart. 2007. "Evaluation of the seismic performance of a code-conforming reinforced-concrete frame building—from seismic hazard to collapse safety and economic losses." *Earthquake Eng. Struct. Dyn.* 36 (13): 1973–1997.
- [19] Jalayer, F., H. Ebrahimian, A. Miano, G. Manfredi, and H. Sezen. 2017. "Analytical fragility assessment using un-scaled ground motion records." *Earthquake Eng. Struct. Dyn.* 46 (15): 2639–2663.
- [20] Jankowiak T, Lodygowski T. Identification of parameters of concrete damage plasticity constitutive model. *Found Civ Environ Eng* 2005; 6: 53–69.
- [21] Jeong, S. H., A. M. Mwafy, and A. S. Elnashai. 2012. "Probabilistic seismic performance assessment of code-compliant multi-story RC buildings." *Eng. Struct.* 34 (Jan): 527–537.
- [22] Kunisue, A. "Retrofitting Method of Existing Reinforced Concrete Buildings Using Elasto-Plastic Steel Dampers." 12th World Conference on Earthquake Engineering (2000).

- [23] Kumar, A., Kumar, A., Kumar, S. K., & Murari, K. (2014). Analysis And Capacity Based Earthquake Resistant Design Of Multi Storeyed Building, 4(8), 7–13.
- [24] Liel, A. B., and G. G. Deierlein. 2013. “Cost-benefit evaluation of seismic risk mitigation alternatives for older concrete frame buildings.” *Earthquake Spectra* 29 (4): 1391–1411.
- [25] Lu, Z. T. 2005. “Application of high performance FRP and innovations of structure engineering.” [In Chinese.] *J. Arch. Civ. Eng.* 22 (1): 1–5.
- [26] Lee J, Fenves G L. Plastic-damage model for cyclic loading of concrete structures [J]. *Journal of Engineering Mechanics Division-ASCE*, 1998, 124(8): 892–900.
- [27] Mohammed A. Sakr, Ayman A. Seleemah, Tarek M. Khalifa, and Galal EL-Samak.” Studying Behavior of Exterior RC Beam–Column Joints Strengthened Using CFRP for Achieving “Strong Column-Weak Beam” In RC Frames”.*East African Scholars J Eng Comput Sci: 2(2) (february-2019)*.
- [28] Miano, A., F. Jalayer, H. Ebrahimian, and A. Prota. 2018a. “Cloud to IDA: A very efficient solution for performing incremental dynamic analysis.” In *Proc., Italian Concrete Days 2016*, edited by M. Di Prisco, and M. Menegotto. New York: Springer.
- [29] Mahdavi, N. and Tasnimi, A. A. “Modeling and verification of response of RC columns strengthened in flexure with mechanically fastened FRP.” *Journal of Vibroengineering* 20 (4) (June 2018).
- [30] Najafgholipour, M. A., Dehghan, S. M., Dooshabi, A. and Niroomandi, A., 2017. Finite element analysis of reinforced concrete beam-column connections with governing joint shear failure mode. *Latin American Journal of Solids and Structures*, 14, pp. 1200-1225.
- [31] Ohu RB (2012) Flexural response of reinforced concrete beams with embedded CFRP plates. Universiti Putra Malaysia, Seri Kembangan.
- [32] Quiertant M, Ferrier E, Chataigner S, Sadone R, Quiertant M, Paris-est U (2012) Anchoring FRP laminates for the seismic strengthening of RC columns. In: *International Conference on Concrete Repair, Rehabilitation and Retrofitting*.
- [33] Paulay, T., & Priestley, M. J. N. (1992). *Seismic Design of Reinforced Concrete and Masonry Buildings*. New York, United States of America (USA).
- [34] Sahoo, R. R. (2008). *Analysis and Capacity Based Earthquake Resistant Design of Multi Bay Multi Storeyed 3D-RC Frame*. Rourkela, Orissa, India.
- [35] Saqan, E. I. (1995). *Evaluation of ductile beam-column connections for use in seismic- resistant precast frames*. PhD thesis University of Texas, Austin.
- [36] Sextos, A., Simopoulos, S., & Skoulidou, D. (2015). *Ductility, Performance and Construction Cost of R / C Buildings Designed to Eurocode 8*, 1–10. Themelis,
- [37] Task Committee on Performance-Based Design “Advocating for Performance-Based Design” Report to the Structural Engineering Institute Board of Governors: ASCE, Structural engineering institute (April, 2018)
- [38] Teng, J. G., J. F. Chen, S. T. Smith, and L. Lam. 2002. *FRP-strengthened RC structures*. Oxford, UK: Wiley.
- [39] Victorsson, V. K. (2011). *The Reliability of Capacity-Designed Components in Seismic Resistant Systems*. Stanford University, California, USA.
- [40] Wang L, Xuan W, Zhang Y, Cong S, Liu F, Gao Q, Chen H (2016) Experimental and numerical research on seismic performance of earthquake-damaged RC frame strengthened with CFRP sheets. *Adv Mater Sci Eng* 2016: 1–11.
- [41] Wang X, Qi Y, Sun Y, Xie Z, Liu W (2019) Compressive behavior of composite concrete columns with encased FRP confined concrete cores. *Sensors (Basel, Switzerland)* 19(8): 1792.
- [42] Ye, L. P., and P. Feng. 2006. “Applications and development of fiberreinforced polymer in engineering structures.” [In Chinese.] *China Civ. Eng. J.* 39 (3): 24–36.
- [43] Zareian, F., P. Kaviani, and E. Taciroglu. 2015. “Multiphase performance assessment of structural response to seismic excitations.” *J. Struct. Eng.* 141 (11).
- [44] Zhang H, Xu X (2019) Comparative analysis of dynamic characteristics of concrete frames reinforced with GFRP Bars and CFRP Bars. In: *IOP Conference Series: earth and environmental science (vol 267)*.
- [45] Zhu, B. L. 1989. *Structural seismic test: Evaluation of seismic performance of structures*. [In Chinese.] Beijing: Seismological Press.